Synthesis, Characterization and Electrochemical Performance of $Li_2Fe_xMn_{1-x}SiO_4$/C as Cathode Material for Thin-Film Lithium-Ion Batteries

A Major Qualifying Project Report

Submitted to the Faculty and Staff of

WORCESTER POLYTECHNIC INSTITUTE

In partial fulfillment of the requirements for the

Degree of Bachelor of Science

By

_____

Andrew Boucher

_____

Michael Ducey

_____

Nathan McNeff

Approvals:

_____

Professor David DiBiasio

Chemical Engineering Advisor

_____

Professor Jianyu Liang

Mechanical Engineering Advisor

Abstract

As technology advances, the need for alternative sources of energy arises. Batteries have been studied by many different research groups as a proper way to power everything from small devices such as cell phones to large units such as cars and factory machinery. Specifically, lithium-ion batteries have been vigorously studied due to their numerous benefits such as high energy density, high voltage and a low self-discharge rate. Thin-film lithium-ion batteries have been researched, but not many successful prototypes have been developed. These prototypes have incorporated active materials such as $LiCoO_2$, $LiMn_2O_4$ and Li_2MSiO_4 (where M=Mn, Fe, Ni, etc.). Based on prior research, many of these materials vary in properties such as theoretical capacity, conductivity and cycling life. Lithium silicates, with two lithium atoms in each molecule, have been proposed as candidates with higher theoretical capacity. Pure phase compounds with a general formula of Li_2MSiO_4 (M=Mn, Fe, Co) have been tested and each has manifested unique drawbacks. In this project we want to test the hypothesis that Li_2MSiO_4 with mixed M of Fe and Mn might provide superior performance to the pure phases as observed in the case of the layered $LiMO_2$ cathodes. We first studied the synthesis of $Li_2Fe_xMn_{1-x}SiO_4$ through a sol gel process. $Li_2Fe_xMn_{1-x}SiO_4$ materials with different Mn to Fe ratios have been synthesized. Carbon coating was used to increase the active material's conductivity. We then characterized the composites through an array of tests, including XRD, SEM and coin-cell battery testing. The results are discussed in this report.

Acknowledgements

Our group would like to thank Professors Jianyu Liang and David DiBiasio for their help and guidance throughout the duration of this project. In addition, we would also like to thank Yinjie Cen, Yuqin Yao and Professor Cunguo Wang whose help was instrumental in the success and completion of our project.

Table of Contents

List of Figures

List of Tables

Executive Summary

Worcester Polytechnic Institute sponsored our project to develop and test different cathode materials for lithium-ion batteries. Current lithium-ion batteries don't have adequate capacity or cycling ability for today's needs, such as smart cell phones and electric cars. Research has been done on some potential cathode materials but each material has met some obstacle that has caused it to not become commercialized. To find a viable cathode material, our group synthesized and analyzed samples of $Li_2Fe_xMn_{1-x}SiO_4$ through SEM, EDX, XRD and electrochemical testing.

We began by collecting data on cathode materials that have been synthesized and thoroughly tested, such as $LiFePO_4$ and $LiMn_2O_4$. Although these two compounds had their own drawbacks, $LiFePO_4$ gave a promising initial capacity and $LiMn_2O_4$ has a high cycling ability. Through further research, we determined that lithium silicate compounds should give a higher capacity than the non-silicate compounds because each molecule will have two lithium atoms. The additional lithium atom means that two lithium atoms will transfer during discharge instead of just one, theoretically doubling the capacity. Unfortunately the silicate compounds are not very conductive, so we had to coat the cathode in carbon. We used a commercial sucrose source to do the carbon coating of the cathode.

Synthesis of the cathode material $Li_2Fe_xMn_{1-x}SiO_4$ was done with a sol-gel process developed in our laboratory. Cathode samples of x=1, 0.7, 0.5, 0.3 and 0 were all created for the purpose of optimizing the material. Samples x=1 and x=0 served as the control for our experiments, as we had found research that had been done on these compounds already. By comparing our data for these samples to the data we found in our literature review we were able to determine that our other samples were comparable to those in the literature review.

The $Li_2Fe_{0.5}Mn_{0.5}SiO_4$ sample was found to have the best initial capacity out of those tested, and also had the best cycling ability. Shown in Figure 1, the 50% sample had an improvement of about 15mAh/g over the 70%/30% sample. The carbon coating severely crippled the capacity of the cathode samples, but it did significantly increase the cycling ability. Scanning electron microscope images showed that the average particle size in all samples was about 400 nm, about 20 times larger than the desired 20 nm. The best results for particle size and morphology were found in the SEM images done for $Li_2Fe_{0.3}Mn_{0.7}SiO_4$. One of the images of $Li_2Fe_{0.3}Mn_{0.7}SiO_4$ is shown in Figure 2. This large particle size limits the capacity of the cathode because it limits the surface area, therefore limiting the theoretical energy density of the particles. We also hypothesized that the commercial sucrose used for carbon coating was inhibiting the pathways needed for a large capacity.

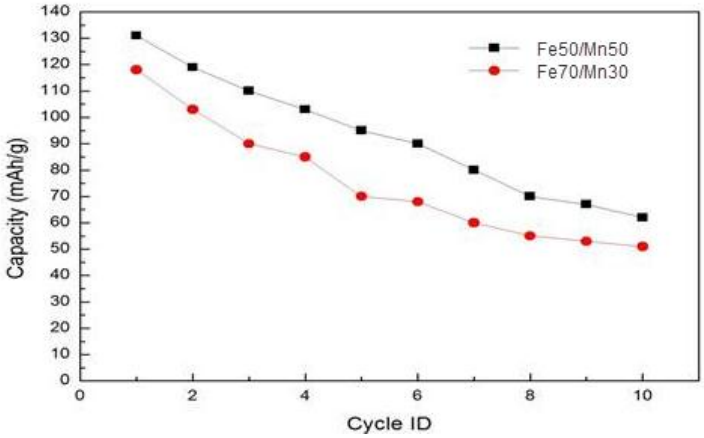

Figure 1: Electrochemical Data for $Li_2Fe_{0.5}Mn_{0.5}SiO_4$ and $Li_2Fe_{0.7}Mn_{0.3}SiO_4$

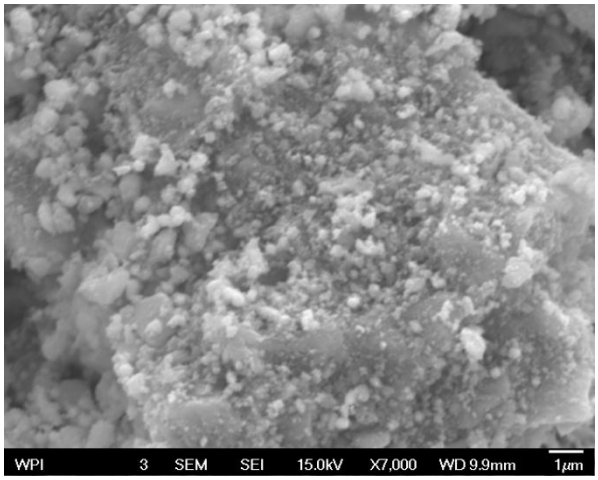

Figure 2: $Li_2Fe_{0.3}Mn_{0.7}SiO_4$ SEM Image

Our recommendations based on our research include a couple changes to our procedure. Instead of using a mortar and pestle to attempt to achieve a particle size of 20 nm, a ball-mill machine could be used. The ball-mill machine should achieve the desired particle size, increasing the theoretical capacity and creating a cathode sample more comparable to commercially used cathode materials. We also recommend using a different carbon source, such as graphene, for carbon coating. This may increase conductivity and cycling ability without compromising the capacity as much.

Chapter 1: Introduction

Batteries have been around since the early 20th century and have provided humans access to electrical power almost anywhere in the world. This has led to many advances in technology and helped to create the "electronic" world we live in today.

Although batteries have been around for over a century, the general mechanism for how they work has remained the same. All batteries are composed of three main components - two electrodes and an ionically conductive material called an electrolyte. The driving force for a battery is a result of the difference in chemical potentials between the two electrodes. These potentials are dictated by the unique chemical compositions of each material. The electrode with the more negative potential is called the anode and the more positive electrode is called the cathode, both of which are connected by the electrolyte. When an external source (i.e. electronic device) is connected to both electrodes, electrons flow spontaneously from the anode to the cathode. The electron flow creates electrical energy which can be harnessed by the external source. (Armand & Tarascon, 2008) In order to maintain the charge balance within the battery, ions are passed through the electrolyte to the electrodes. Some batteries have the unique ability to be recharged by applying a voltage in the opposite direction from cathode to anode. The energy density of any battery is a direct function of its voltage and capacity. (Armand & Tarascon, 2008)These two variables are completely dependent upon the chemical makeup of each battery component and the way all the components interact as a unit. It is this search for the perfect chemical interactions that has given rise to our project. (Armand & Tarascon, 2008)

The lithium-ion battery was first introduced to the consumer market in 1991 (Nishi, Lithium Ion Secondary Batteries; Past 10 Years and the Future, 2001) by Sony Corporation. Many other companies then followed suit, and the market share for the lithium-ion battery began to grow exponentially. Lithium-ion batteries have spurred the creation of many portable devices such as iPods, cell phones and

laptops. The ability to recharge the battery coupled with the large capacity and long lifespan has made the lithium-ion battery a huge success in the consumer markets. (Buchmann, 2008)

The future holds many opportunities for lithium-ion batteries. Electric cars are doing testing with lithium-ion batteries right now to see how well the batteries will perform in that setting. (Zhang, et al., 2001) The United States government has created a department named the Advanced Technology Department (ATD) which is intended to assist the development of lithium-ion batteries for use in electric cars. Electric cars are slowly being introduced to the United States right now, and as the number of electric cars increases so will the market for lithium-ion batteries.

Printable electronics are a technology that holds great promise for the near future. Electronics will be printed onto a substrate using an inkjet or LaserJet printer that are standard in any household today, using specialized materials in place of the ink. (Leenen, Arning, Thiem, Steiger, & Anselmann, 2009) By using organic materials instead of the materials (mostly metals) used in electronics today it will make the electronics much cheaper to produce, which will result in a lower price tag for consumers. (Fan, et al., 2009) The limits of technology will be remarkably broadened, with devices such as flexible displays, sensor tapes and artificial skin.

These recent developments in the field of batteries are powerful revelations that may change the abilities of batteries in the near future, but many batteries, especially lithium-ion batteries, have similar drawbacks that need to be improved upon. Poor cycle performance is one of the common problems with all batteries. (Tarascon J.-M. , 2010) With poor cycle performance, batteries will not last as long as the first time they are used and will slowly decrease their capacity on every recharge of the battery. A long charging time is also necessary for most batteries making it difficult to have uses for current batteries in items like cars that need quick recharges for people on the go (a 1 hour commute home from work could turn into several hours). (Nishi, Lithium Ion Secondary Batteries; Past 10 Years

and the Future, 2001) Poor safety characteristics are a main concern of lithium ion battery users also. (Nishi, Lithium Ion Secondary Batteries; Past 10 Years and the Future, 2001) These concerns are rooted in the fact that current lithium ion batteries will have chemical changes inside the battery over the course of the battery's lifetime that need to be addressed. One last problem with lithium ion batteries is the problem of high electronegative differential causing low energy efficiency. (Tarascon M. A.-M., 2008)

Thin film batteries and different material/electrolyte chemistries are common cures for many of the problems with current lithium ion batteries. Many problems are rooted in lithium dendrites forming inside the battery. These dendrites will form from lithium deposits on the anode and cathode of a battery that will eventually penetrate the separator and cause the battery to short circuit, which can cause a fire due to the oxidizing component of the battery. (Nishi, Lithium Ion Secondary Batteries; Past 10 Years and the Future, 2001) These dendrites are also the cause of poor cycle life because if the lithium is depositing somewhere other than back into the chemical makeup of the electrodes, and then it is no longer usable in the battery. A solution to these problems is to change the chemical makeup of the electrodes to be more willing to have a reversible chemical reaction which would allow for the lithium ions to be accepted back into their original electrode and not deposit elsewhere causing dendrites. Coating of the nanoparticles in a thin film battery has been a step already taken to improve the effectiveness of the electrodes. The coatings for these electrodes are commonly carbon and along with increasing the conductivity of the materials, it helps with preventing internal corrosion of the electrodes and electrolyte, increasing the cycling and safety of the batteries. (Tarascon M. A.-M., 2008) The thin film also allows for faster charging of the batteries due to the high surface area of the electrodes allowing faster transfer of electrons to reverse the internal reaction of the battery. Electrolytes are another component of the battery that can have chemical research to discover the effectiveness of different types of phases and chemical makeup in a lithium ion battery.

Despite the possibilities for developing the thin film lithium ion batteries, there has not been sufficient progress in the field. Much of this is due to the lack of resources. The materials used in these batteries are not found from renewable resources, but from ores. These components need to be mined which make them very expensive and, like oil, have the potential to run out in the near future. (Tarascon M. A.-M., 2008) For example, if all cars in the near future are running on lithium batteries, approximately 30% of the world's lithium will be used up. Despite this fact, there is almost unlimited lithium that can be found in the water, but the means to extract it involves high energy consumption causing the cost of useable lithium to be very expensive. (Tarascon M. A.-M., 2008) Not only is the extraction of the lithium expensive, but the fabrication of lithium based electrodes involves high energy costs also. (Tarascon M. A.-M., 2008) Along with expensive costs to use lithium, the nanoparticles that make up the thin film of the electrodes are known to have a very low packing density lowering the energy density of the potentially powerful batteries, (Tarascon M. A.-M., 2008) forcing studies to increase packing density before the rest of the battery can be developed.

The traditional cathode materials used in today's the Li-battery industry are a group of 3-d transition metal oxides like $LiCoO_2$, $LiNiO_2$ and $LiMnO_4$. However, the major downfall of these materials lies in their ability to only accept/extract one Li-ion per 3-d transition metal. Orthosilicates, like our material $Li_2Fe_xMn_{1-x}SiO_4$, have the potential to transfer two Li-ions per 3-d transition metal. (Tarascon J.-M. , 2010) In theory, this should double the capacity of Li-ion batteries. (Islam, Dominko, Masquelier, Sirisopanaporn, Armstrong, & Bruce, 2011) The key feature which sets orthosilicates apart from their metal oxide counterparts is their tetrahedral structure. This structure provides stability in the lattice while creating the necessary "space" to allow for the insertion/de-insertion of two Li-ions per 3-d transition metal. It has been shown that when the life cycle of Li_2FeSiO_4 is compared to that of Li_2MnSiO_4, the Li_2FeSiO_4 has much better stability and capacity retention. However, when the initial capacity of Li_2MnSiO_4 is compared to that of Li_2FeSiO_4, Li_2MnSiO_4 has much greater potential. (Islam,

Dominko, Masquelier, Sirisopanaporn, Armstrong, & Bruce, 2011) The goal of our project is to create a compound of $Li_2Fe_xMn_{1-x}SiO_4$ that combines the stability in lattice structure and cycling behavior seen in $Li_2FeSiO_4$with the potential capacity of Li_2MnSiO_4.

The goal of our project is to synthesize a cathode material composed of $Li_2Fe_xMn_{1-x}SiO_4$ that has an increased capacity and cycling life. To do this, we will develop a procedure which can produce compounds of $Li_2Fe_xMn_{1-x}SiO_4$ with varying amounts of Mn and Fe. Each unique compound will be characterized using SEM and XRD to reveal the structural properties of the material. Similarly, the capacity and cycling life of each compound will be discovered through electrochemical testing. Based upon the results of the electrochemical testing we will be able to suggest the optimum ratio of Mn and Fe in the $Li_2Fe_xMn_{1-x}SiO_4$ cathode material.

In chapter 2, the background section, we will demonstrate the relevance and importance of our research through a literature review. Chapter 3 contains our methodology which describes the steps taken to reach our goal. Chapter 4 discusses the data obtained from our analysis and Chapter 5 then talks about the relevance and application of this data. Additional figures and data can be found in the Appendices.

Chapter 2: Literature Review

This section serves as a summary of the extensive literature review that we performed for this project. It is separated into sub-sections discussing different aspects of the lithium-ion battery.

2.1 Li-ion Batteries in the Market

The lithium-ion battery was first introduced to the consumer market in 1991 (Nishi, Lithium ion secondary batteries; past 10 years and the future, 2001) by Sony Corporation. Many other companies then followed suit, and the market share for the lithium-ion battery began to grow exponentially. Lithium-ion batteries have spurred the creation of many portable devices such as iPods, cell phones and laptops. The ability to recharge the battery coupled with the large capacity and long lifespan has made the lithium-ion battery a huge success in the consumer markets. (Buchmann, 2008)

The future holds many opportunities for lithium-ion batteries. Electric cars are doing testing with lithium-ion batteries right now to see how well the batteries will perform in that setting. (Zhang, et al., 2001) The United States government has created a department named the Advanced Technology Department (ATD) which is intended to assist the development of lithium-ion batteries for use in electric cars. Electric cars are slowly being introduced to the United States right now, and as the number of electric cars increases so will the market for lithium-ion batteries.

Printable electronics are a technology that holds great promise for the near future. Electronics will be printed onto a substrate using an inkjet or LaserJet printer that are standard in any household today, using specialized materials in place of the ink. (Leenen, Arning, Thiem, Steiger, & Anselmann, 2009) By using organic materials instead of the materials (mostly metals) used in electronics today it will make the electronics much cheaper to produce, which will result in a lower price tag for consumers. (Fan, et al., 2009) The limits of technology will be remarkably broadened, with devices such as flexible displays, sensor tapes and artificial skin that will be made possible.

2.2 Li-ion Battery Mechanism

Batteries operate by emitting stored energy in the form of electricity. The energy stored is in the form of electrons in the anode of the battery. Releasing energy comes from a completed circuit that allows the battery to reach equilibrium by releasing ions from the anode to pass through the electrolyte and react with the cathode. While this process takes place, the electrons from the anode are released into the circuit and passed to the cathode to allow the full reaction of the ions. The battery runs out of power when all of the ions are used up and the battery has reached equilibrium. Recharging the battery involves reversing the reaction by forcing electrons back into the battery to release the electrolyte's ions from the anode back into the cathode. In the case of lithium ion batteries, the ion being passed through the electrolyte is a lithium (+1) ion, which is stored in the cathode as a mixture with different materials that are appropriate for the needs of the battery.

Capacitors are similar to batteries in their function, but operate using a much different mechanism than a battery. Capacitors are able to recharge and release energy much faster than a battery, but store much less energy. Thin-film batteries have qualities of both a capacitor and a battery, allowing for rapid electricity release, shorter battery recharge time, and high energy storage. A thin film battery has these capabilities, but they can be altered by changing the chemical formula and the size of the film. (Coxworth, 2011)

The cathode of the thin film lithium ion battery is vital to the transfer of lithium ions in the battery, and participates in the exchange electricity in a circuit. The volume is one of the most important aspects of the cathode. The surface area that results due to creating a thin film of a cathode is what allows for high energy transfers. Surface area translates into contact area with the electrolyte, and more contact area means that there are more places for the chemical reaction in the battery to take place. The electrolyte acts as an intermediate for transport of the lithium ions to the electrode, but without proper contact area, the transference of ions greatly decreases; but the surface area is not the

sole reason for this large transference of energy. The lithium ions are a large part of the high energy transfer also due to the ions being so small. With small ions, the material can be much denser and have more ions in a smaller area than other battery cathodes causing a much higher energy density, and when combined with the thin film, there is a massive amount of energy in a very small area. This concept is what gives the thin batteries their ability to transfer large amounts of energy at high speeds compared to normal batteries currently used in common practice.

The transfer of electrons does not happen immediately when the anode touches the electrolyte. There must be a complete circuit for electrons to flow for a full reaction to take place. Most batteries operate using an oxidation/reduction reaction, which is controlled by the available amount of electrons, such as the following reaction in battery:

$$LiCoO_2 \leftrightarrow Li_{1-x}CoO_2 + xLi^+ + xe^-$$

Once this type of reaction for the given battery is ready to react, the battery will produce a current. The power of the current is controlled by the contact area of the electrodes with the electrolyte. This surface area allows for high voltage because of the speed of the reaction. Higher contact area leads to higher ability for the ions to react. The chemical reaction takes place where the electrolyte touches the anode, which forces the lithium ions out of their host compound for transfer to the cathode.

Before the lithium ions are produced, they are in a host compound known as the anode. To make these useable ions, there needs to be the ability

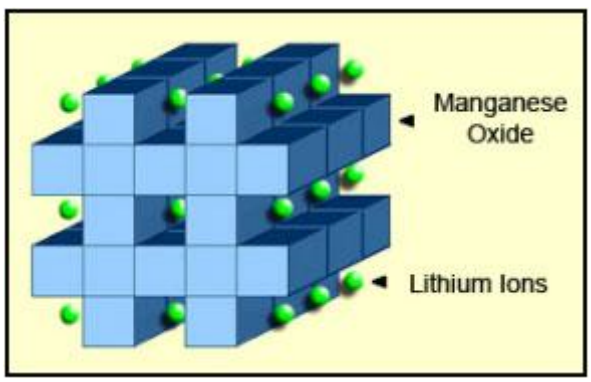

Figure 3: $LiMn_2O_4$

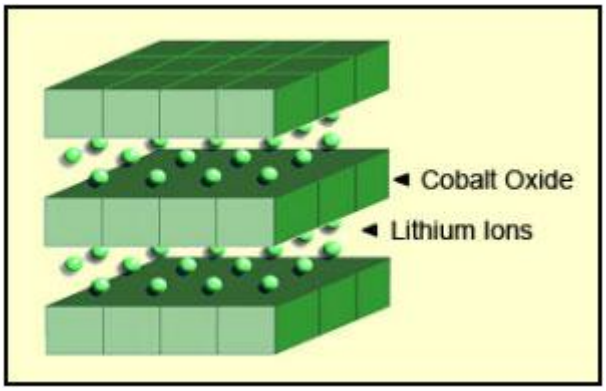

Figure 4: $LiCoO_2$

to chemically react. This requires the ability for electrons to flow from one reactant (the anode) to the other (the cathode) (as shown in the sample reaction above) and the ability for the two reactants to transfer ions. The transfer of electrons takes place through the circuit and the ions travel through the electrolyte. For the ions to travel through the electrolyte, they need to be readily accepted by the cathode. The lithium is readily accepted because of the structure of a lithium ion battery cathode. The chemical structure of a lithium ion cathode is crystallized in layer or rows, as shown in Figure 3 and Figure 4. These layers consist of either a spinel or, in the case of Figure 3, an oxide and lithium ions. The lithium ions can also form in rows within a matrix of a spinel or an oxide; such is the case in Figure 4.

When the cathode material is synthesized, it forms a matrix of the spinel or oxide that makes up the compound and the lithium ions fill the holes in the matrix that are not already occupied by the lithium ions that are in the cathode material. The creation of the spinel matrix happens due to the affinity for spinel to form in alternating tetrahedral shapes that share oxygen atoms; such is shown in Figure 5, while the atomic structure is shown in Figure 6.

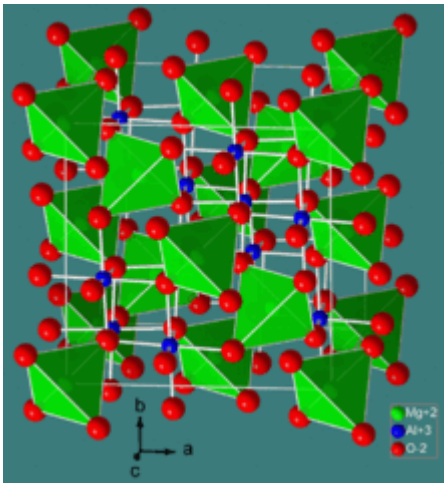

Figure 5: General Tetrahedral Crystallization with Intermediate Ions Unit Cell View

To cause the reaction to be possible the anode has to have readily reactable lithium. Due to the nature of lithium in its atomic form, it is willing to surrender one of its electrons so that the outer shell of the ion is balanced. Many lithium ion batteries use carbon and silicon, which has currently come to people's attention, so that the anode can form in structures that will support atomic lithium. (American Physical Society, 2011)

The use of an anode may be opposite to that of a cathode, but the design is similar. The anode needs to be able to support atomic lithium; therefore it must be structured much like that of the cathode. Graphite (carbon with a sheet-like structure) has been used as a cathode is because the lithium atoms are able to be held between the sheets of carbon. Another way to store atomic lithium is by coating it onto the anode, allowing for the surface to have readily available lithium for the chemical reaction. (American Physical Society, 2011)

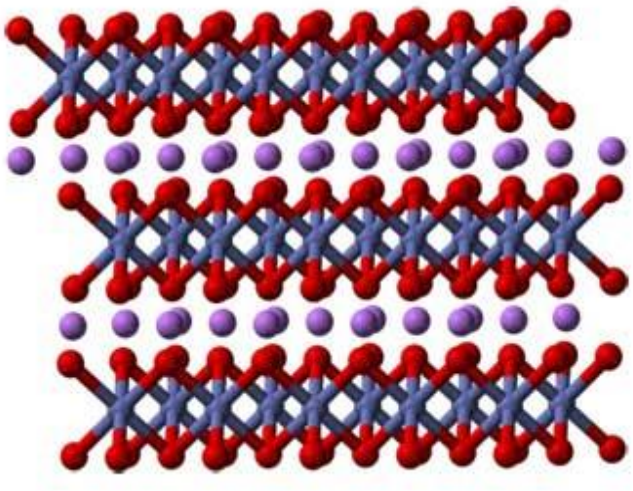

Figure 6: General Tetrahedral Crystallization with Intermediate Ions Lateral View

This need for readily available lithium in the anode also develops the need for high surface allowing for high surface contact with the electrolyte. There are some materials that have a high surface area, such as lithium titanium oxide which creates a jagged looking surface as nanoparticles. This jagged surface creates a surface area that is up to one hundred times the area of average materials used in average lithium ion battery anodes.

2.3 Common Materials

Given that lithium-ion batteries have such a large market share, there are a number of commonly used materials for the various parts of the battery. This section discusses those materials, as well as the benefits and drawbacks of some of them.

2.3.1 Electrolyte

Despite the large amounts and speeds of energy transfer that is possible with thin film lithium ion batteries, one of the main reasons thin film batteries are wanted at the consumer level is the safety.

To make a thin film battery, solid state electrolytes are a requirement because the thin films used to make the battery cannot contain a liquid electrolyte. This element of safety comes from the electrolyte being solid, so that if the battery corrodes or is punctured, the corrosive or flammable liquid electrolyte used in most other batteries, does not leak.

One of the main types of solid state electrolytes being researched are glassy solids made of either polymers or ionic bonded materials. The most widely used solid state electrolyte for thin film batteries was developed in Oak Ridge National Laboratory in the early 1990's and has some of the best ionic conductivity of any solid state electrolyte created. This electrolyte is lithium phosphate as a glass with nitrogen, technically called lithium phosphorous oxynitride, and now known as Lipon. The nitrogen is the key part to the electrolyte, and it becomes part of the structure by replacing some of the oxygen in the material. This addition of nitrogen allows for a large increase in ionic conductivity, even in small amounts. If the nitrogen to oxygen ratio is only 0.1, the ionic conductivity of the lithium glass will increase 40 fold. One of the big advantages to the use of Lipon comes from the lack of reactivity. Lipon will not react with metallic lithium or degrade at high temperatures. Not reacting with metallic lithium is key for an electrolyte because most of the thin film batteries have been lithium based with a metallic lithium anode, and the electrolyte is the barrier between the anode and cathode. Despite all the great qualities of this Lipon, there exists a downside. Lipon is one hundred times less conductive than a regular liquid electrolyte battery, but this is overcome by the electrolyte being much slimmer than that of the liquid electrolyte; Lipon will be used at proximately one to three micrometers thick. (Dudney N. J., 2008)

Another inorganic solid state electrolyte used is thio-LISICON, which stands for Lithium Superionic Conductor. The formula is generalized by "Li_xM_{1-y} M'_yS_4 (M = Si, Ge, and M'= P, Al, Zn, Ga, Sb)" (Christopher P. Rhodes, 2010) and is synthesized at different compositions using different

temperatures to achieve different crystal structures. Different forms of this electrolyte have been known to produce the highest ionic conductivity of any solid state, inorganic electrolyte at over 10^{-3} S/cm. After subjecting the thio-LISICON to a planetary ball milling process, the ionic conductivity will increase to even higher levels, along with large electrochemical windows. The main reasons thio-LISICON is not used in thin film batteries now is because the production process still needs to be refined to make the process cheaper and the formula has to be optimized for the best results. (Christopher P. Rhodes, 2010)

Oxide based inorganic electrolytes are another form of electrolyte that has been looked at be labs as a possible improvement on the lithium ion battery. For oxide based electrolytes to be effective, they need to have large enough pathways in the lattice for lithium ions to pass through and some disorder in the sublattice of the structure. These compounds are also considered LISICONs but they are oxide based instead of sulfide based. One of the successful electrolytes that was developed is $Li_{3.6}Ge_{0.6}V_{0.4}O$ which was recorded to have an ionic conductivity of 4×10^{-5} S/cm, which is exponentially less than that of thio-LISICON, but still usable. The oxide based electrolyte that has been found to have the same qualities as thio-LISICON is known as lithium lanthanum titanate ($Li_{3x}La_{(2/3)-x}TiO_3$). Oxide compounds have also been mixed into a solid solution to create an amorphous or glassy electrolyte. Li_2O-V_2O_5-SiO_2 is the system that is a good example of the glassy type of electrolyte, which displays acceptable qualities such as 10^{-5} S/cm for ionic conductivity and negligible electronic conductivity. (Iriyama)

A type of thin-film battery that uses solid state electrolytes is known as a quasi-thin solid-electrolyte battery. This type of battery incorporates the use of polymer based electrolytes as plastics and glasses. These electrolytes show that they have potential use for thin batteries due to maintaining performance above the glass transition temperature, and remaining stable after hundreds of cycles, but

the electrolytes are approximately sixty to one hundred fifty micrometers. With these qualities, this electrolyte combines both large bulk batteries and thin film batteries. The disadvantage to these types of electrolytes come from the fact that they do not conduct ions as well as needed for such a large battery, making them highly inefficient. (Solid State Thin-Film Battery Systems, 1999)

2.3.2 Cathode

To incorporate the solid state electrolyte properly into the battery's system, there needs to be proper cathode material. The research in this area has developed an increase of approximately 8-10% in battery capacity every year, showing that the cathode material is slowly developing, but have room for much more improvement. (Targray, 2011) One potential material that has been worked on is lithium titanate, $Li_4Ti_5O_{12}$. Lithium titanate, also known as LTO, creates the desired crystalinity that is desired for lithium ion batteries, forming in the tetrahedral crystals that are lined up in sheets, creating space for lithium ions to diffuse into the lattice. The electrical capacity of this material is 175mAh/g and has a voltage of 1.5V. LTO is one of the safer cathode materials and has excellent cycle life, but one of the best advantages to this material is the extremely high power that is available. The chemical formula of LTO is $Li_4Ti_5O_{12}$, but when is it fully used up (has accepted as many lithium ions as it possibly can), the formula then becomes $Li_7Ti_5O_{12}$. This large increase in lithium allows for the large capacity, but the surface area is where the power comes from. LTO has a surface area that is very jagged compared to most other materials, allowing up one hundred times more surface area in the same unit of space. This surface area allows for the transferring lithium ions to react much faster with this cathode than any other cathode currently developed and the surface area becomes even greater when the material is created as nanoparticles. Despite the large amount of ion transfer that takes place with LTO, the volume of the material will only increase up to 0.2% of the

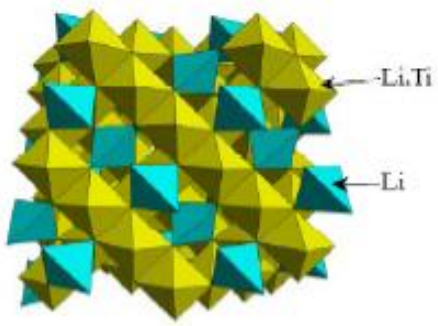

Figure 7: Lithium Titanate

original volume, allowing it to be very structurally sound. The largest and only major downside to this material is the poor temperature performance, and with the speeds that the ion transfer takes place in an LTO cathode, low temperature performance is the downfall of this type of cathode. (Patterson, 2009)

One of the most widely studied cathode materials is $LiMn_2O_4$. Lithium manganese oxide has similar qualities to that of LTO. It has a jagged surface, increasing the surface area significantly compared to many other cathode materials. This large surface area combined with a small grain structure, allows for fast diffusion through the material. Lithium manganese oxide exhibits a maximum capacity of 62.4µAh/cm*µm and will run between 3.0 and 4.5V. The main advantage to this cathode is the cycle life, the battery can be recharged up to 500 times at 55°C and still keeps its crystal structure showing that it has better thermal resistance than that of LTO which is a much more powerful cathode. (Lu, 2006)

Silicon has also been studied as a cathode material. In theory, silicon is one of the best cathode materials that can be used; it has a theoretical capacity of 4200mAh/g. Silicon can also be used to create higher capacity batteries or lighter batteries, but will increase in volume by 300% when fully reacted with lithium because each silicon atom can take four lithium atoms. This size increase is a problem due to the fact that most cathodes will not expand as drastically, even graphite, which is commonly used as a cathode, will increase by only 10%. The large inflation also will make silicon structurally unstable and fall apart mechanically; having silicon in nanoparticles helps to solve this problem and increases the cycle life, but does not eliminate the problem completely due to silicon not being in stabilized rows of atoms like most other cathodes. Despite the downsides to silicon, if silicon is incorporated into a spinel with lithium and other metals,

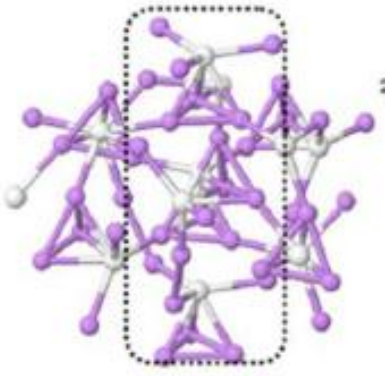

Figure 8: Lithium-Silicon Crystallization
White= Silicon
Purple=Lithium

the expansion may not happen, but there is the possibility that high capacity will be kept. (Patterson, 2009)

2.4 Characterization

Characterization is the process involved with revealing the unique features of a material. In the case of an unknown or new substance, characterization is important for two reasons. First, the identity of the unknown substance can be determined by comparing the key features of a known substance to that of the unknown. Secondly, characterization allows for correlations to be made between the specific features of a material and its physical properties. The second capability of characterization can help direct research in the future by suggesting which material characteristics are required to produce a desired physical property. The two techniques discussed below aim to study the material on an atomic level. These techniques are scanning electron microscopy and x-ray powder diffraction.

2.4.1 Scanning Electron Microscopy

A scanning electron microscope (SEM) is used to observe and characterize material at the nanometer to micrometer scale. One key feature of this device is its ability to produce three-dimensional-like topographic images. It does so by sweeping a finely focused electron beam in a raster across the surface of the specimen. The resulting contact between the electron beam and sample produces many types of imaging signals. The three most commonly used are secondary electrons, backscattering electrons and characteristic x-rays. Variations in the secondary and backscattering electrons reveal changes in elevation (topography) on the surface of the sample. The image created from these signals has a large depth of field and the contrast between the two signals is responsible for the three-dimensional appearance of the image. Another capability of the scanning electron microscope is its ability to analyze the composition of a specimen. By using the characteristic x-rays produced from the electron beam-specimen interaction both qualitative identification and quantities elemental information can be obtained. (Goldstein, et al., 2003)

All SEM's, like the human body, are an interconnected network of subsystems that work together to produce an image. These subsystems can be categorized according the two major components in which they are found, either the electron column or the control console. Located at the top of the column is an electron gun which is used to generate electrons and accelerate them at the sample with energy in the range of 0.1-30 keV. Before the electrons produced from the gun are allowed to interact with the sample, they are passed through a series of two or more electron lenses to demagnify the electron beam and place a much smaller focused electron spot on the specimen. Most SEMs are capable of producing an electron beam with a spot size less than 10 nm. The electron beam is swept across the specimen by two pairs of electromagnetic deflection coils. This motion forms a rectangular "raster" on the specimen which the scan generator simultaneously replicates on the viewing screen. The magnification of the image is the ratio of the length of the raster on the viewing screen to the length of the raster on the specimen. For example, a 10 μm wide raster on the specimen that is displayed on a 10 cm wide viewing screen will produce a 10,000x magnification. In order to increase the magnification, the scan coils are less strongly excited causing the electron beam to deflect across a smaller distance on the specimen (reducing the width of the specimen's raster). The electron detector collects the signals produced from electron beam-specimen interaction and converts them to point-by-point intensity changes. Contrast in the image is formed from variations in the signals collected at different points along the raster. The standard Everhart-Thornley detector collects both secondary and backscattering electrons by applying a voltage (both positive and negative) to the collector screen in front of the detector. When a positive voltage is applied, both types of signals are collected. However, when the screen collector receives a negative voltage the low-energy secondary electrons are repelled, leaving only the backscattering electrons to be captured. Once the electrons are collected by the scintillator/photomultiplier they are amplified for viewing on the cathode ray tube screen. The cathode ray tube viewing screen is a major component of the control console, as well as various controls used for

adjusting different parts of the column (i.e. electron gun, lens strength, working distance and aperture size). (Goldstein, et al., 2003)

There are four parameters which affect the image produced on the cathode ray tube viewing screen - the electron probe (spot) size, the electron probe current, the electron probe convergence angle and the electron beam accelerating voltage. For clarification purposes the definition of each parameter is described below: The electron probe size refers to the diameter of the final electron beam at the surface of the specimen. The electron probe current is the final current of the electron beam at the surface of the specimen. The electron probe convergence angle is defined as the half-angle of the cone of electrons converging onto the specimen. The electron beam accelerating voltage is a defining characteristic of the electron gun.

Resolution refers to the size of the smallest details that can be observed. In order to obtain a useful image the probe diameter must be at least, if not smaller, than the feature being examined. Therefore a high resolution image is produced from the smallest possible probe size with sufficient beam current to exceed the visibility threshold. To obtain an image with maximum clarity, large beam currents are required. Even if the spot size is smallest enough to be easily resolved, details cannot be observed without sufficient beam current. Large beam currents are also necessary for x-ray microanalysis. The electron beam convergence angle affects the depth of field of an image. When the beam angle is low, the beam diameter changes only slightly over a long vertical distance, allowing surface features of different heights to be in focus at the same time. Operating an SEM at low electron beam accelerating voltages provides and image which is rich in surface detail. When the voltage is increased the beam penetrates deeper into the specimen, decreasing the amount of surface information available. However, although low voltages provide enhanced surface detail this may reduce the

resolution of the image. In order to obtain an image of desired quality each of these parameters must be adjusted concurrently. (Goldstein, et al., 2003)

2.4.2 X-ray Powder Diffraction

X-ray powder diffraction is non-destructive technique to analyze a material based upon its crystal structures and atomic spacing. X-rays are made to contact the specimen at a range of different angles and the diffraction intensities are measured for each. Every crystalline structure for every chemical compound has a unique diffraction pattern. The International Center Diffraction Data (ICDD) maintains a database of all known diffraction patterns. These known patterns can be compared to an unknown specimen to identify the substance.

X-rays are a form of electromagnetic radiation with a wavelength of approximately 1 angstrom, about the same size as the typical distance between atoms in a crystalline solid. In 1912, Max von Laue discovered that this characteristic of x-rays makes them particularly well suited for studying the atomic spacing and crystal structure of a substance. (Dutrow & Clark, 2011) When an x-ray beam contacts an atom it interacts with the atom's electrons. The result of this interaction alters the path of the x-rays, much like waves in the ocean "diffracting" off an island rock. In almost all directions the diffracted x-rays from each atom will combine and effectively cancel each other out (destructive interference). However, when all the atoms are arranged in a periodic fashion (definition of a crystal), in certain directions, the interferences will combine (constructive interference) to produce a diffracted x-ray beam. (Chapter 7: Basics of X-ray Diffraction, 1999) W.L. Bragg and his father developed an equation to relate the wavelength of the beam to the diffraction angle and the lattice spacing in a crystalline sample. The equation is as follows:

$$2dsin(\theta) = n\lambda$$

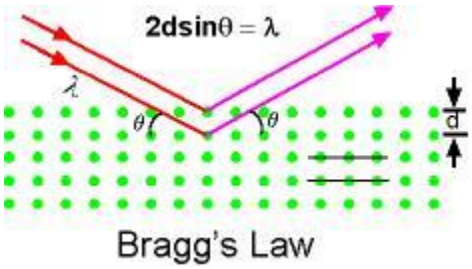

Figure 9: Bragg's Law

Where d is the inter-plane distance between lattice planes, theta is the scattering angle, n is an integer representing the order of the diffraction peak and lambda is the wavelength of the x-ray. (Introduction to X-ray Diffraction) When Bragg's law is satisfied, a constructive interference occurs resulting in a peak in intensity at the corresponding two theta angle. Using this information, key features of the crystal lattice are revealed.

X-ray diffractometers consist of three main components- an x-ray tube, a sample holder, and an x-ray detector. Inside the x-ray tube, a voltage is applied to a filament to accelerate electrons at the specimen. To produce the monochromatic x-rays needed for diffraction the electron beam must be filtered by foils or crystal monochrometers. The theta compensating slit collimates the x-rays before they reach the specimen. In x-ray powder diffraction, the specimen is ground up into a fine powder of randomly oriented single crystals. This powder is then placed into the sample holder which is rotated at an angle of theta with respect to the collimated x-ray beam. The scintillation counter (x-ray detector) measures the diffracted x-ray intensity and is mounted on a motorized arm which rotates at an angle of two theta with respect to the x-ray beam. The instrument used to maintain the angle and rotate the sample is termed a goniometer. When the geometry of the incident x-rays contacting the specimen satisfies the Bragg equation, constructive interference occurs resulting in a peak in intensity. For typical powder patterns, data is collected at two theta angles between 5 and 70 degrees. (Dutrow & Clark, 2011)

2.5 Electrochemical Testing

The voltage of any galvanic cell is fixed by the electrochemical characteristics of the active chemical compounds used. To determine a battery's performance capabilities, the interaction of these active chemicals are studied under a variety of different conditions. These test help to reveal the ideal application for the battery.

Cycle life is a key performance parameter for batteries which indicates the expected working lifetime of the cell. It is defined as the number of cycles a cell can perform before its capacity drops to 80% of its initial specific capacity. During each charge and discharge cycle the materials in the cell slowly deteriorate, causing a continual decline in capacity. This is may be due to unavoidable chemical actions in the cell or a change in morphology of the particles making up the electrodes. In both cases there is a reduction in volume of the active chemicals which increases the cell's internal impedance and decreases its capacity. (Battery Performance Characteristics, 2005)

2.6 Areas of Improvement

The development of thin-film lithium-ion batteries has been occurring for over twenty years. Batteries that are capable of withstanding high temperatures of up to 260°C has driven research towards discovering a working thin-film lithium-ion battery. (Bates, Dudney, Neudecker, Ueda, & Evans, 2000) Micro scale lithium-ion batteries have been created, but not any that fulfill all the needs of the consumer market. Batteries that don't include a lithium-ion electrode have been tested, but they don't possess the rechargeability or capacity that lithium-ion batteries have. (Neudecker, Dudney, & Bates, 2000)

According to Tesla Motors, the electric car is the way of the future, not hybrids or fuel cell cars. (Eberhard & Tarpenning, 2007) The discovery of a viable thin-film lithium-ion battery will be a crucial step in getting electric cars on the road. Donald Sadoway, a professor at MIT, was interviewed to talk about the debate between using batteries or fuel cells in future generations of cars. He said the main

reason people still aren't buying electric cars is the fuel range, not being able to drive more than 70-100 miles on one charge. By continuing the research on thin-film lithium-ion batteries, Sadoway said: "I think we could easily double [the energy capacity of] what we have right now. We have cells in the lab that, if you run the numbers for a thin-film cell of reasonable size, you end up with two to three times current lithium ion [batteries]." (Bullis, 2005) Sadoway said that his driving desire to create thin-film lithium-ion batteries comes from a desire to get rid of the internal combustion engine in cars. He said that by creating a viable electric car, greenhouse gas emissions will decrease and our impact on the Earth will be reduced. (Bullis, 2005) Sadoway also talked about fuel cell technology, stating that it is an effective energy source but the requirement of hydrogen ions will be the downfall of the technology. In order to split the H_2 a platinum or palladium catalyst must be used, and the price of these metals is too great to legitimize fuel cell use. As Sadoway put it, "Lithium right now is probably $40 a pound. Platinum is $500 an ounce. If I could give the fuel-cell guys platinum for $40 a pound, they would be carrying me around on their shoulders until the day I die." (Bullis, 2005)

Cars use lead-acid batteries now for startup, lighting and ignition purposes. Not only are these batteries inefficient, but they are harmful to the environment when they are disposed. By developing lithium-ion batteries to perform these tasks, environmental impact will be reduced. More specifically, thin-film lithium-ion batteries are a viable replacement to the lead-acid batteries because of their greater capacity and rechargeability compared to traditional lithium-ion batteries. (Petrovic, 2011) Batteries in cars will also need to be safe because things like car accidents could cause the batteries to become dislodged. (Jansen, et al., 1999)

Alternative energy sources to burning carbon, such as solar panels and wind turbines, have an increasing need for an efficient electrical energy storage (EES) device. (Datta, et al., 2011) Lithium-ion batteries are the leading technology currently being researched to be an EES, but better capacity and

rechargeability are needed before lithium-ion batteries are utilized. Thin-film lithium-ion batteries promise an increase in both battery properties previously mentioned, and therefore is the next logical step to be an EES. The decreased space needed for the thin-film batteries will also be helpful, as it will give the designers more flexibility (both figuratively and literally) while they create the layout for the EES of the future.

The desire for thin-film lithium-ion batteries derives mostly from a need for higher energy density and power density in devices. As new technology is discovered, the trend is for that technology to need more power than its predecessor. Technology is also showing a trend of becoming smaller, which parallels the need for smaller energy sources that provide more power than their larger counterparts. (Liu, Li, Ma, & Cheng, 2010)

Other desires for thin-film lithium-ion battery technology come from the toxicity of some lithium-ion batteries currently in use. In Li_xCoO_2 batteries, the toxicity of cobalt is raising some eyebrows, along with the high price and limited abundance of the metal. (Kim, et al., 2008) The use of manganese, iron and silicon works much better than cobalt, with much higher abundance, lower costs and lower toxicity. The increased effectiveness of these materials promises an improved lithium-ion battery that utilizes the benefits of each metal while minimizing the negative effects.

Another aspect of the thin-film lithium-ion battery that needs improvement is the material used as an electrolyte. The substances used today lack the surface area needed to efficiently transport electricity from a thin-film battery. By using an amorphous carbon coating as the electrolyte, the surface area in contact with the electrodes is maximized while the electricity is efficiently transported from the anode to the cathode. (Liu, Li, Ma, & Cheng, 2010) However, an effective way to evenly carbon coat the cathode and anode material has still not been developed. The heat used in the carbon coating

process can cause agglomeration of the nanoparticles, reducing the surface area and therefore the efficiency of the battery. (Liu, Li, Ma, & Cheng, 2010) (Datta, et al., 2011)

Chapter 3: Methodology

This section details the steps that were taken to synthesize and test the cathode material $Li_2Fe_xMn_{1-x}SiO_4$.

3.1 Cathode Synthesis

In order to determine the silicate based composite with the best electrochemical performance, samples with varying ratios of iron and manganese were synthesized. Five different ratios of iron to manganese were used: 0/1, 0.3/0.7, 0.5/0.5, 0.7/0.3 and 1/0. The mass of each chemical precursor is shown in the table below and was calculated using 5mL of tetraethyl orthosilicate (TEOS) as the basis.

Table 1: Mass Requirements for Cathode Synthesis

$Li_2Fe_xMn_{1-x}SiO_4$	x=0	x=0.3	x=0.5	x=0.7	x=1
manganese acetate tetrahydrate	0 g	7.55g	12.55 g	17.59 g	25.14 g
ferrous oxalate dihydrate	4.06 g	2.84 g	2.03 g	1.22 g	0 g
lithium acetate dehydrate	4.6g	4.6g	4.6g	4.6g	4.6g

Stoichiometric amounts of ferrous oxalate dehydrate (Alfa Aesar, 99%) and manganese acetate tetrahydrate (Alfa Aesar, Mn 22%) were mixed according to the ratios specified above. Under nitrogen (AIMTEK, 99.999%) flux and constant stirring, the iron and manganese compounds were dissolved in 20mL of ethanol (see lab setup diagram below). 5mL of tetraethyl orthosilicate (Aldrich, Reagent Grade, 98%) was added dropwise to the solution. In a separate beaker, 4.6g of lithium acetate dehydrate (Alfa Aesar, 99%) was dissolved in 20mL of ethanol. All components of the composite were combined by adding the lithium solution dropwise to the beaker containing the iron and manganese (still under nitrogen flux). To initiate the formation of the sol, 0.5mL of deionized

water and 1.5mL of acetic acid were added dropwise to the solution. The solution was stirred continuously overnight until the gel was formed. Once formed, the gel was transferred from the beaker to a ceramic boat and heated in the tube furnace (Thermolyne 79300) under nitrogen flux at 80^{o}C for 24 hours. After all the solvent in the gel's pores had been evaporated during the heating process, the dried composite was removed from the tube furnace and ground using a ceramic pestle and mortar. From this point on in the procedure, the sample can be carbon coated or tested in its unaltered form. For carbon coating, see the procedure below. The resulting powder was pressed into a pellet using a crimping machine (MSK-110) set to apply a force of 20,000 lbs_f for 2 minutes. The pellet was then calcinated in the tube furnace under nitrogen flux at 700^{o}C for 10 hours. To create the desired crystal structure, the tube furnace was set to a heat rate of 10^{o}C per minute until a temperature of 300^{o}C was reached. After this point the heat rate was reduced to 2^{o}C per minute. The pellet was removed from the furnace and ground using a pestle and mortar. The resulting powder was mixed at a weight ratio of 80: 10: 10 with a poly(vinylidene fluoride) (binder)(Alfa Aesar)/N-methyl-2-pyrrolidene (Sigma-Aldrich, 99.5%) solution and carbon black (Alfa Aesa, 99%+). The slurry was then sprayed onto an aluminum foil (Alfa Aesar, 99.9%) current collector. To evaporate all excess solvent, the current collector was placed into a vacuum furnace at 120^{o}C for 10 hours. This newly created cathode material was combined with a pure lithium (Alfa Aesar, 99.9%) anode, lithium hexafluorophosphate electrolyte (Syerm Chemicals, INC, 99.9%+) and a commercial grade polypropylene separator (Celgard$^{@}$ 2500) inside a (CR2032) coin cell shell. The assembly of the test coin cell was performed in a vacuum hood. The cell's initial capacity and cycling life performance at a discharge/recharge rate of 0.1C for 20 cycles was tested using a MTI-EQ-BST8-10MA battery test station.

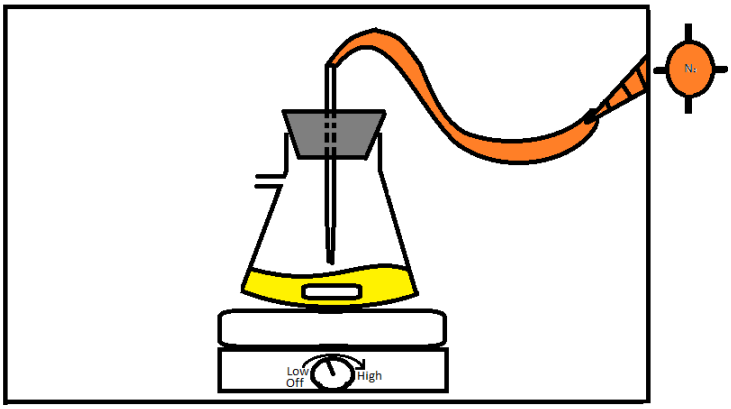

Figure 10: Cathode Synthesis Lab Setup

3.2 Carbon Coating

To carbon coat the precursor, the powder formed after grinding the dried out gel is mixed with 10% weight commercial sucrose (Great Value) and dissolved in 15mL of acetone. To evaporate all the acetone, the solution is heated in the box furnace for 24 hours at 80^{o}C. Once all the solvent has been evaporated, the carbon coated sample is ground using a pestle and mortar. The same procedure for the calcination and coin cell assembly steps were followed as described above.

3.3 Characterization

To reveal the particle size, distribution and morphology the powder sample was analyzed using a JSM – 7000F scanning electron microscope (SEM). The microscope was operated at an acceleration voltage of 15 kV and a working distance 10mm. The energy dispersive x-ray detector (EDX) feature of the microscope was utilized to confirm the presence of all elements in the composite.

The crystal structure of the material was analyzed by an X'PERT POWDER (PANalytical Co.) x-ray diffractometer. The non-carbon coated calcinated powder sample was inserted into the sample

holder and scanned from 15° to 80° with Ge-monochromatized Cu $K\alpha_1$ radiation of 0.154059nm in wavelength.

Chapter 4: Results and Analysis

This section discusses the results obtained from testing and analysis done on the synthesized cathode samples as well as the carbon coating data.

4.1 Carbon Coating

Based on analysis of the SEM and EDX images, 8wt% carbon coating had the least amount of carbon coating and did not have the desired conductivity expected. 12wt% carbon coating had the most amount of carbon applied to the surface, but it was very inconsistent, spanning from 18wt%-60wt%. The 12wt% samples did achieve the desired conductivity for the material, but significantly dropped the initial capacity. 10wt% carbon coating was much more consistently applied to the test material than the 12wt% samples. 10wt% samples also had moderate electrochemical results, increasing the conductivity much more than 8wt% samples and not decreasing the capacity as much as the 12wt% samples. The carbon coating had two results that were consistent with all the samples. The similarities consisted of large increases in conductivity compared to the samples without carbon and large decreases of initial capacity in all the samples.

4.2 Cathode Synthesis

The synthesis of the cathode was the focal point of the research that was done. Samples of the cathode yielded results that ranged from the structure of the molecules to the size of the particles and the initial capacity of each compound. The following section provides summaries of the results that were drawn from the testing discussed in the literature review section, with more detailed results in the appendices.

4.2.1 SEM Analysis

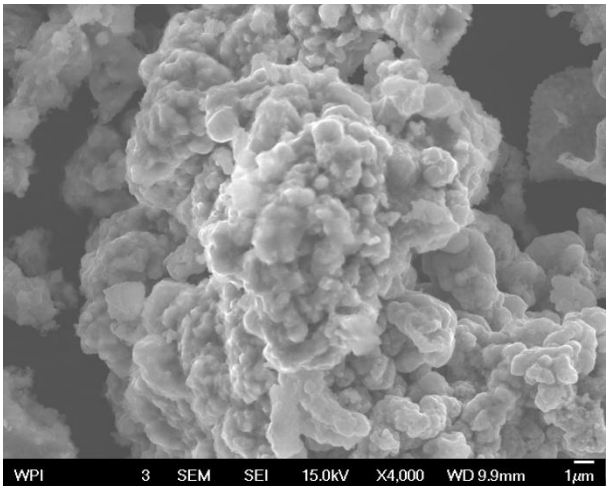

Figure 12: Li_2MnSiO_4 SEM Image 1

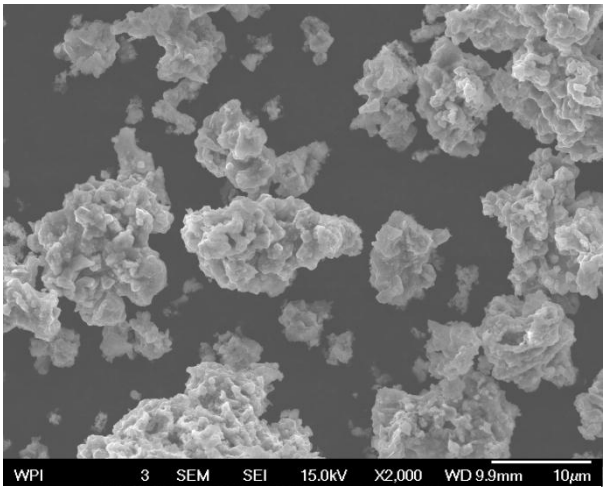

Figure 11: Li_2MnSiO_4 SEM Image 2

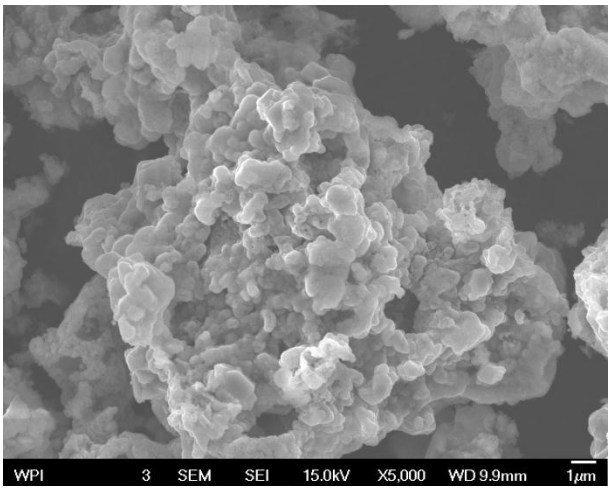

Figure 13: Li_2MnSiO_4 SEM Image 3

Figures 11-13 are SEM images of Li_2MnSiO_4 or the sample referred to as 0wt%Fe/100wt%Mn. These images are magnified 2000-5000 times to show the crystal size and the morphology of the particles. The particle size is in a range of several hundred nanometers to a few micrometers. The particles are clumped together to form larger amorphous particles, but the smaller particles are rounded, slightly amorphous particles. The particles are larger than the 20-50 nanometer diameter particles desired for the results of this experiment and leads to hybridizing Li_2MnSiO_4 and Li_2FeSiO_4.

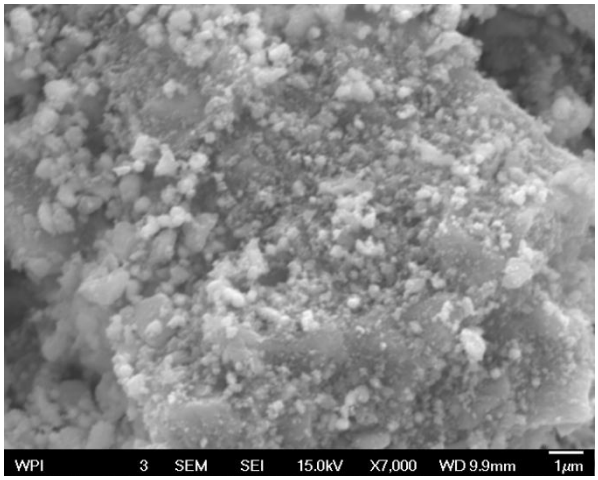

Figure 15: $Li_2Fe_{0.3}Mn_{0.7}SiO_4$ SEM Image 1

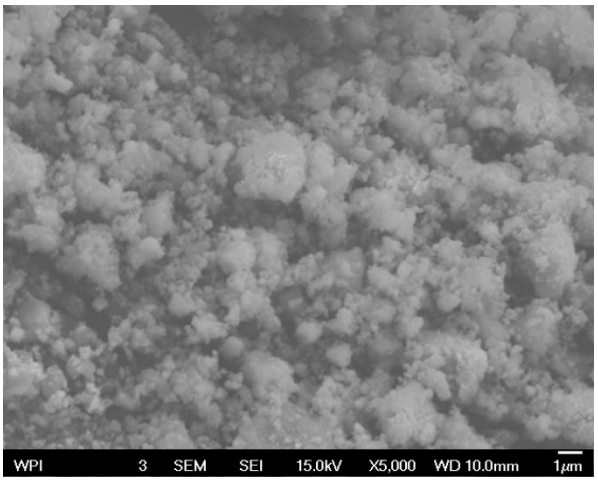

Figure 14: $Li_2Fe_{0.3}Mn_{0.7}SiO_4$ SEM Image 2

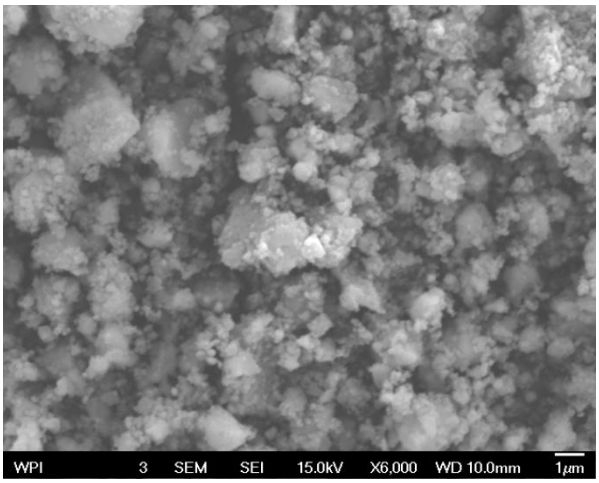

Figure 17: $Li_2Fe_{0.3}Mn_{0.7}SiO_4$ SEM Image 3

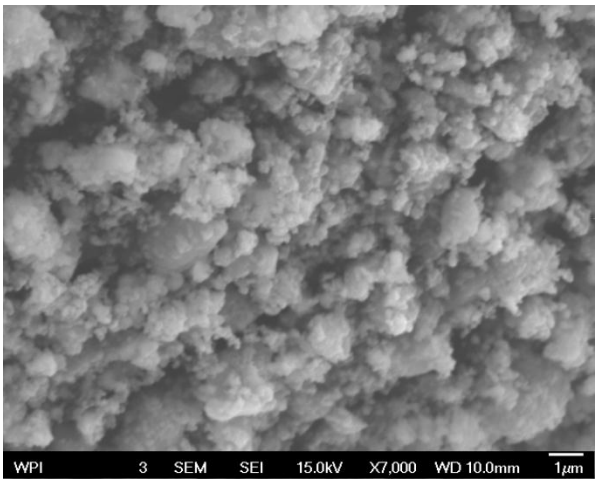

Figure 16: $Li_2Fe_{0.3}Mn_{0.7}SiO_4$ SEM Image 4

Figures 14-17 are SEM images of $Li_2Fe_{0.3}Mn_{0.7}SiO_4$ or the sample referred to as 30wt%Fe/70wt%Mn. These images are magnified 5000-7000 times to show the crystal size and the morphology of the particles. As shown, all particles range from tens of nanometers to a few micrometers. Most of the particles are approximately a few hundred nanometers in diameter which is above the desired size. The morphology of the particles is generally spherical, but there are amorphous particles mixed into the material.

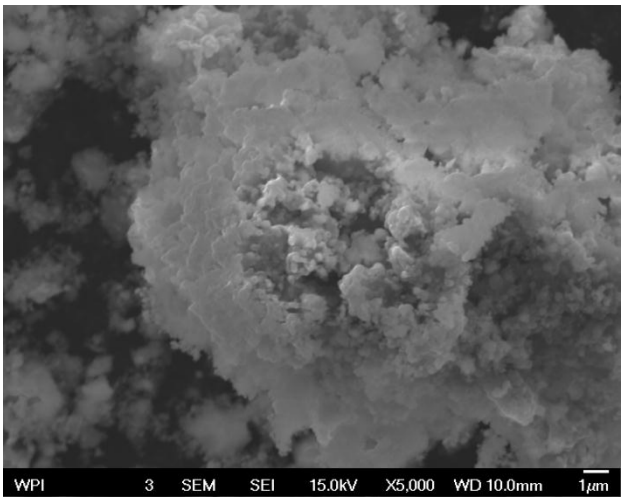

Figure 19: $Li_2Fe_{0.5}Mn_{0.5}SiO_4$ SEM Image 1

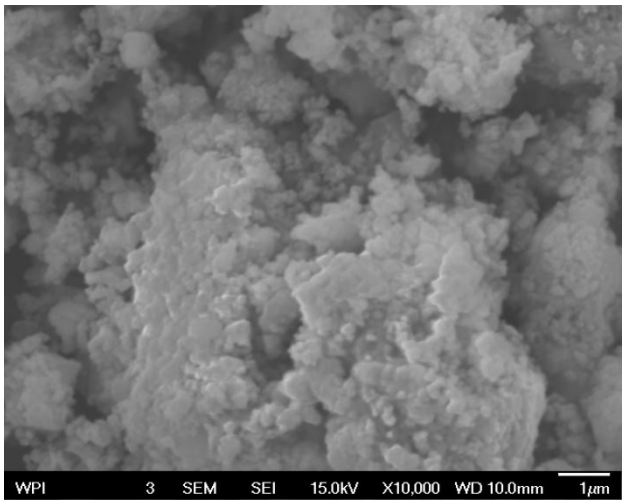

Figure 18: $Li_2Fe_{0.5}Mn_{0.5}SiO_4$ SEM Image 2

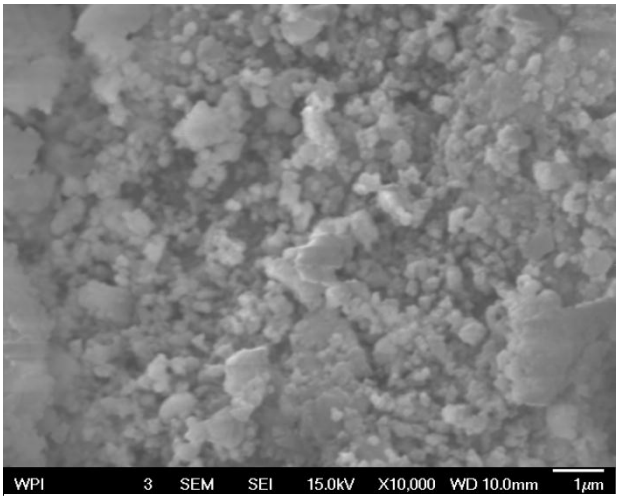

Figure 20: $Li_2Fe_{0.5}Mn_{0.5}SiO_4$ SEM Image 3

Figures 18-20 are SEM images of $Li_2Fe_{0.5}Mn_{0.5}SiO_4$ or the sample referred to as 50wt%Fe/50wt%Mn. These images are magnified 5000-10,000 times to show the crystal size and the morphology of the particles. The particle size ranges from approximately 100 nm to several micrometers in diameter. Most of the particles are approximately 300-500 nm, which is greater than the desired particle size. The morphology of the smaller particles is spherical, but the larger particles are sheeted and appear to be remaining in a dendritic formation, possibly due to a lack of proper processing of the material. The sheeted particles are not desired in the final product due to their low surface area.

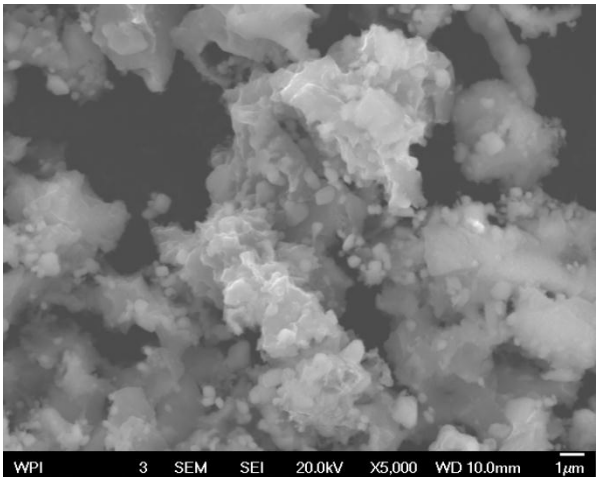

Figure 22: $Li_2Fe_{0.7}Mn_{0.3}SiO_4$ SEM Image 1

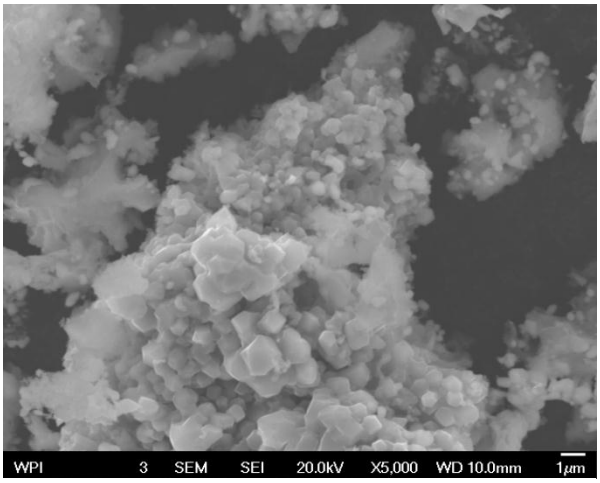

Figure 21: $Li_2Fe_{0.7}Mn_{0.3}SiO_4$ SEM Image 2

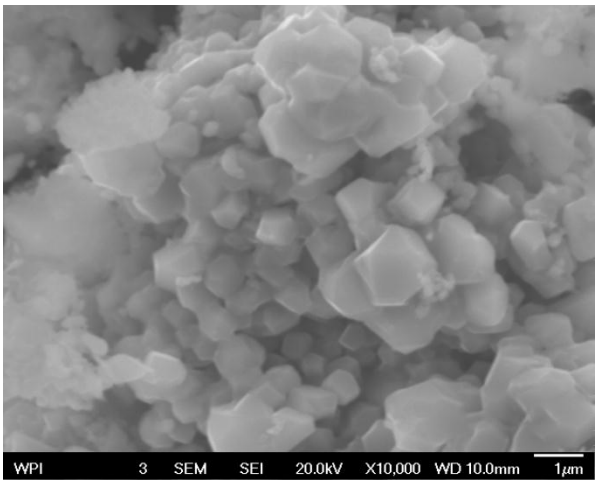

Figure 23: $Li_2Fe_{0.7}Mn_{0.3}SiO_4$ SEM Image 3

Figures 21-23 are SEM images of $Li_2Fe_{0.7}Mn_{0.3}SiO_4$ or the sample referred to as 70wt%Fe/30wt%Mn. These images are magnified 5000-10,000 times to show the crystal size and the morphology of the particles. The particles are in a range of 200 nanometers to 2 micrometers. Most of the particles are approximately 500 nanometers, which is larger than the desired diameter for the particles. The shape of the particles is consistent with that of a cube which may have formed due to lack of proper processing after the synthesis.

The images of the hybridized variations of the cathode have much smaller particles than that of the original Li_2MnSiO_4. The size difference in the particles increases the amount of surface area inside of the cathode material, potentially causing a much greater charge transference and initial capacity. The morphology is consistent in each sample except for $Li_2Fe_{0.7}Mn_{0.3}SiO_4$ which is cube shaped instead of spherical.

4.2.2 XRD Analysis

As was discussed in the literature review, the XRD analysis reveals the crystal structure of the synthesized lithium compounds. The -olivine crystal structure is the desired result of the synthesis, as it will be the one that can use two lithium atoms per molecule during charge and recharge.

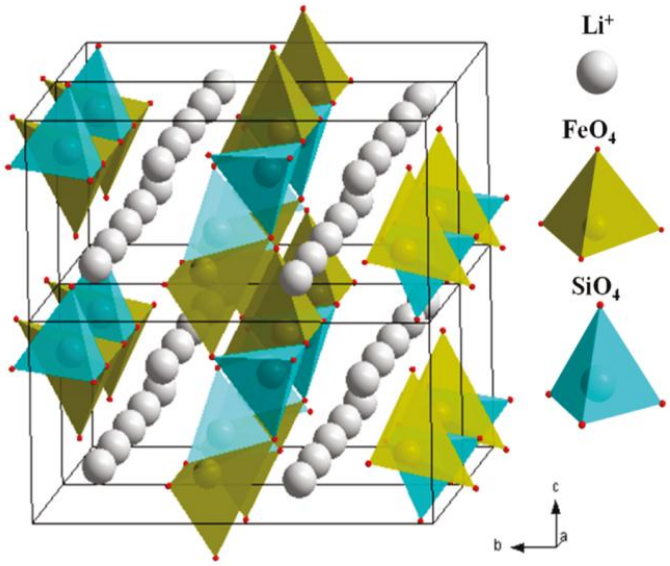

Figure 24: Olivine Crystal Structure

Figure 24 shows the desired olivine crystal structure for the cathode material. As can be seen in the figure, the lithium atoms are suspended between the tetrahedrally stacked metals, making it easier to remove and replace them during the aforementioned charge and discharge processes.

The XRD analysis gives a graph that plots intensity as a function of the x-ray angle, and it reveals the structure of the compounds through peaks and valleys. Using the XRD patterns obtained from a literature review as the basis for analysis, it was determined that the desired crystal structure was obtained during cathode synthesis.

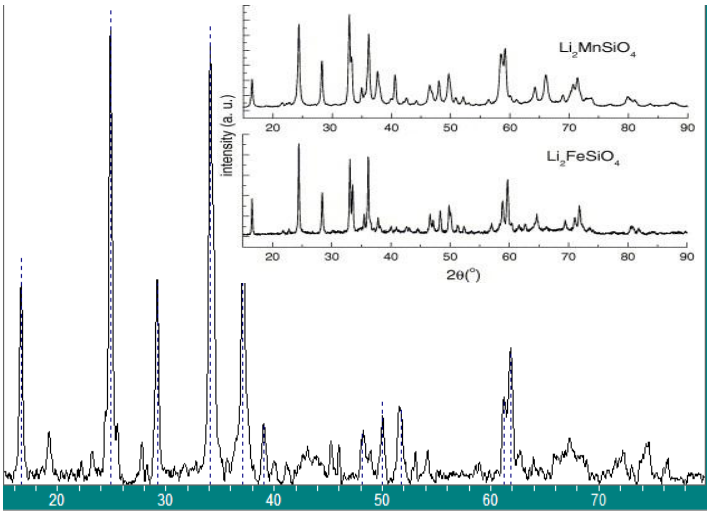

Figure 25: XRD Pattern of $Li_2Fe_{0.5}Mn_{0.5}SiO_4$

The XRD pattern of $Li_2Fe_{0.5}Mn_{0.5}SiO_4$ is shown in Figure 25 along with XRD patterns of Li_2MnSiO_4 and Li_2FeSiO_4. The pattern of the 50/50 compound was obtained through XRD analysis of a cathode sample synthesized through the methodology listed previously. Both the manganese and iron compounds have XRD patterns that were obtained through literature review. The peaks on the pattern from the hybrid molecule match the peaks on both the manganese and iron molecule patterns, proving that the structure of the hybrid molecule synthesized using the procedure listed in the methodology is similar to the structure of the two pure compounds.

4.2.3 Electrochemical Testing

The electrochemical testing was done to measure both the initial capacity and the cycling performance of 10% carbon coated cathode samples. As was discussed in the methodology, the electrochemical analysis was done using the coin-cell procedure. After the coin-cell was assembled, it was connected to a machine that can monitor charge and discharge into the cell. The machine takes data on the

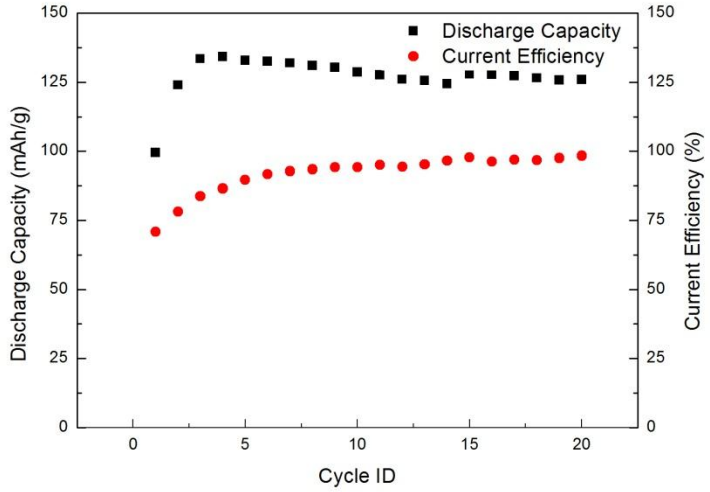

Figure 26: Li2Fe0.7Mn0.3SiO4/C Coin-Cell Data

capacity of the cell each time it is discharged, which gives the initial capacity on the first discharge and then by plotting the capacity of each discharge the cycling ability of the battery can be found. As can be seen in Figure 26, the initial capacity of the coin-cell is about 100 mAh/g, while the maximum capacity can be found on the third cycle at about 135 mAh/g. The cycling ability can be seen by looking at the loss of capacity between the maximum capacity achieved by the cell and the capacity of the final cycle. For this cell, the capacity goes from the max of 135 mAh/g to about 125 mAh/g, a loss of about 7.4% capacity in 20 cycles.

The cycling ability shown by the previous sample was much better than the samples that were not carbon coated. In Figure 27, the two samples were charged and discharged without the carbon coating. The initial capacity is shown to be similar to the carbon coated sample, with the 50/50 sample having an initial capacity of approximately 133 mAh/g and the 70/30 sample having an initial capacity of approximately 120 mAh/g. Without the carbon coating, the capacity of the samples drops drastically with each cycle, resulting in a 51.9% loss in the Fe50/Mn50 sample and a 58.3% loss in the Fe70/Mn30 sample in just ten cycles. Further electrochemical data obtained from coin-cell analysis can be found in Appendix B.

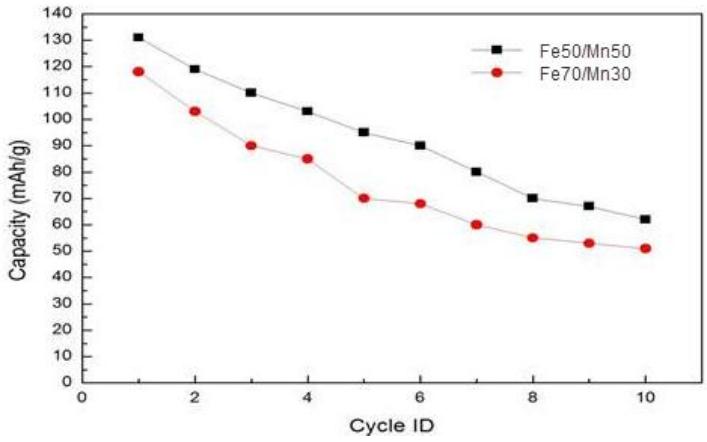

Figure 27: Fe50/Mn50 and Fe70/Mn30 Coin-Cell Data

Chapter 5: Conclusions and Recommendations

Based on the carbon coating analysis found in Appendix A, 10wt% carbon coating was chosen for the optimal amount. 8wt% carbon coating was too little carbon coating and did not achieve the desired electrochemical specifications. 12wt% carbon coating had the most amount of carbon applied to the surface, but it was very inconsistent, spanning from 18wt%-60wt%. This inconsistency created unpredictability in the potential products created. The 12wt% samples did achieve the expected conductivity for the material, but dropped the initial capacity more than desired. 10wt% carbon coating was much more consistently applied to the test material than the 12wt% samples. 10wt% samples also had the best electrochemical properties out of the three tests. The potential for a more consistent carbon coating could be solved using a more pure form of carbon such as graphene. The carbon was formed using commercial sucrose which needed to be heated to break carbon away from the sucrose molecule. This heating could have caused agglomeration of particles, creating a larger particle size than what could have been achieved otherwise.

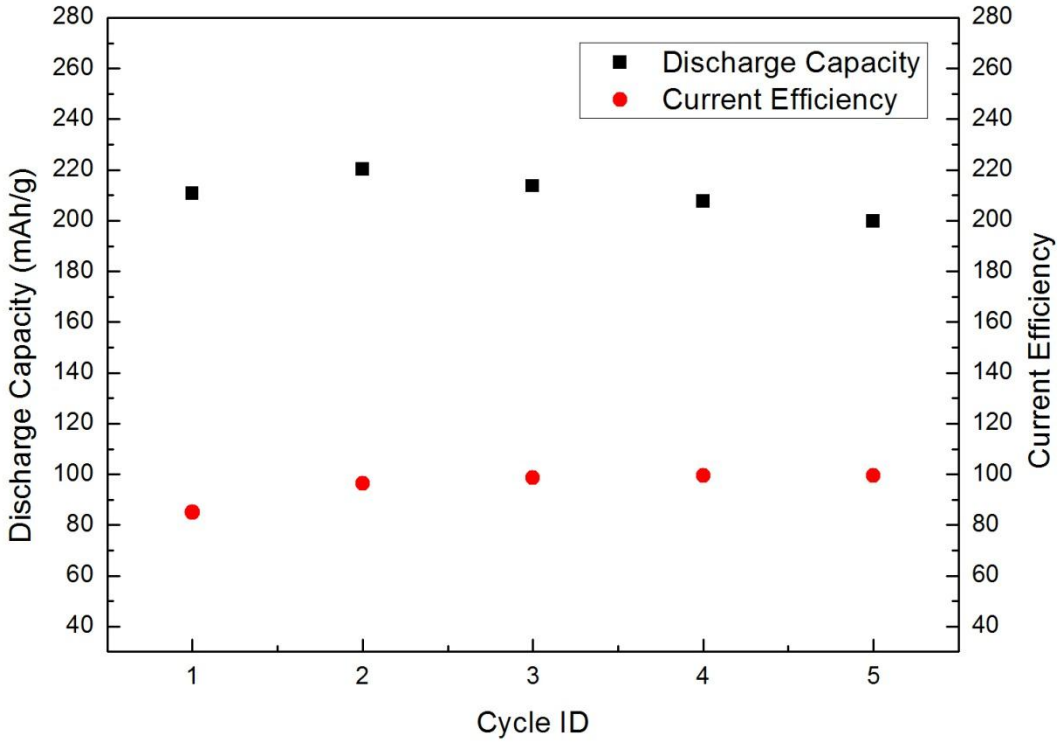

Figure 28: $Li_2Fe_{0.7}Mn_{0.3}SiO_4$ with Graphene Electrochemical Testing

Electrochemical testing was done for $Li_2Fe_{0.7}Mn_{0.3}SiO_4$ with carbon coating done using graphene. The results are shown in Figure 28. At 210 mAh/g and then 220 mAh/g the initial capacity was higher than any other sample tested, both carbon coated and non-carbon coated. Conductivity can explain this phenomenon, as it allows for better flow of electrons and results in higher current because of it. The cycling ability was also improved over the non-carbon coated samples, with a loss of 9% capacity over five cycles. Although the cycling ability was not as high as when the sample was coated with sucrose, this was only a preliminary test and the graphene coating remains very promising.

Different samples of the cathode were successfully created; the samples being $Li_2Fe_{0.7}Mn_{0.3}SiO_4$, $Li_2Fe_{0.5}Mn_{0.5}SiO_4$, $Li_2Fe_{0.3}Mn_{0.7}SiO_4$, and Li_2MnSiO_4. Based on SEM imaging of the samples, the best particle size and morphology came from the $Li_2Fe_{0.3}Mn_{0.7}SiO_4$ samples, which produced the smallest particle size and a similar particle shape throughout the material. All the samples had a similar problem with their size, the particles were too large. The particle size desired was a range of 20-50 nanometers in diameter and the minimum diameter across all the samples was approximately 200 nm. The particle size and morphology problems in the samples could be solved by a better processing technique than grinding the samples using a pestle and mortar. Ball milling is an option for better processing which would result in smaller particles increasing surface area and therefore, capacity. Ball milling can also break apart the irregular crystals shapes.

The electrochemical testing was done for the samples of $Li_2Fe_{0.5}Mn_{0.5}SiO_4$ and $Li_2Fe_{0.7}Mn_{0.3}SiO_4$ with and without carbon coating. The results showed that both compounds have similar initial capacity and cycling ability. $Li_2Fe_{0.5}Mn_{0.5}SiO_4$ had slightly better results for the initial capacity with and without carbon coating, so it is recommended that the 50wt%Fe/50wt%Mn sample be used when electrochemical results are considered. Testing should be done with the 50wt%Fe/50wt%Mn sample with graphene carbon coating to see if it is an improvement over the initial results shown by the 70wt%Fe/30wt%Mn sample.

X-Ray Diffraction analysis based on comparison of the XRD pattern of the hybridized samples to the XRD pattern of $LiMnSiO_4$ and $LiFeSiO_4$ shows the structural pattern of the crystalline samples. $Li_2Fe_{0.5}Mn_{0.5}SiO_4$ was found to have a similar XRD pattern proving that it has the desired crystal structure making it a feasible option as a cathode material. Assuming the desired crystal structure is similar throughout all the samples, due to the process being identical and similar particle size, it can be determined that the best ratio from our results is 50wt%Fe/50wt%Mn. There is

potential that $Li_2Fe_{0.3}Mn_{0.7}SiO_4$ could have better electrochemical results, but the data is not available at this time.

The final recommendation is that these materials are studied more in depth while using graphene as the carbon coating, which could lead to a cathode with better properties than most cathodes on the market.

Works Cited

Chapter 7: Basics of X-ray Diffraction. (1999). Retrieved December 20, 2011, from http://epswww.unm.edu/xrd/xrdbasics.pdf

Battery Performance Characteristics. (2005). (Woodbank Communications Ltd) Retrieved 1 12, 2012, from Electropaedia: http://www.mpoweruk.com/performance.htm

Targray. (2011). Retrieved November 2011, from http://www.targray.com/li-ion-battery/cathode-materials/cathode-active-materials.php

American Physical Society. (2011). *Lithium Ion Batteries: Delivering a Charge*. Retrieved November 16, 2011, from http://www.physicscentral.com/explore/action/lithium-1.cfm

Armand, M., & Tarascon, J. (2008). Building Better Batteries. *Nature*, 652-657.

Bates, J. B., Dudney, N. J., Neudecker, B., Ueda, A., & Evans, C. D. (2000). Thin-film lithium and lithium-ion batteries. *Solid State Ionics*, 33-45.

Buchmann, I. (2008, September). *Will Lithium-Ion batteries power the new millenium?* Retrieved November 6, 2011, from Batteries in a Portable World: http://www.buchmann.ca/Article5-Page1.asp

Bullis, K. (2005, November 22). *The Lithium Economy.* Retrieved November 30, 2011, from Technology Review: http://www.technologyreview.com/NanoTech/wtr_15920,318,p1.html

Christopher P. Rhodes, Y. F. (2010). *Solid-State Lithium Batteries Using thio-LISICON Solid-State Electrolytes*. Retrieved Novemeber 2011, from https://www.ornl.gov/ccsd_registrations/battery/abstracts/Solid-state%20batteries_abstract_Rhodes_2010-08-30.pdf

Coxworth, B. (2011). *New Battery Technology May Allow For Complete Recharge Within Minutes.* Retrieved November 8, 2011, from gizmag.com: http://www.gizmag.com/3d-thin-film-batteries-recharge-in-minutes/18187/

Datta, M. K., Maranchi, J., Chung, S. J., Epur, R., Kadakia, K., Jampani, P., et al. (2011). Amorphous silicon-carbon based nano-scale thin film anode materials for lithium ion batteries. *Electrochimica Acta*, 4717-4723.

Dudney, N. J. (1999, October). *Solid State Thin-Film Battery Systems.* Retrieved November 2011, from Science Direct: http://www.sciencedirect.com/science/article/pii/S1359028699000522

Dudney, N. J. (2008). *Thin Film Micro-Batteries.* Retrieved November 2011, from www.electrochem.org: http://www.electrochem.org/dl/interface/fal/fal08/fal08_p44-48.pdf

Dutrow, B. L., & Clark, C. M. (2011, February 1). *X-ray Powder Diffraction*. Retrieved December 20, 2011, from Geochemical Instrumentation and Analysis: http://serc.carleton.edu/research_education/geochemsheets/techniques/XRD.html

Eberhard, M., & Tarpenning, M. (2007, April 17). *The 21st Century Electric Car*. Retrieved 11 28, 2011, from Tesla Motors: http://www.fcinfo.jp/whitepaper/687.pdf

Fan, Z., Ho, J. C., Takahashi, T., Yerushalmi, R., Takei, K., Ford, A. C., et al. (2009). Toward the Development of Printable Nanowire Electronics and Sensors. *Advanced Materials*, 3730-3743.

Goldstein, J., Newbury, D., Joy, D., Lyman, C., Echlin, P., Lifshin, E., et al. (2003). *Scanning Electron Microscopy and X-Ray Microanalysis* (3rd ed.). New York, New York: Springer Science+Business Media, Inc.

Introduction to X-ray Diffraction. (n.d.). (National Science Foundation) Retrieved December 20, 2011, from Materials Reseatch Laboratroy at UCSB: http://www.mrl.ucsb.edu/mrl/centralfacilities/xray/xray-basics/index.html

Iriyama, Y. (n.d.). *A Novel All-Solid-State Thin-Film-Type Lithium-Ion Battery with In-Situ Prepared Electrode Active Materials*. Retrieved November 2011, from http://www.intechopen.com/source/pdfs/10411/InTech-A_novel_all_solid_state_thin_film_type_lithium_ion_battery_with_in_situ_prepared_electrode_active_materials.pdf

Islam, M. S., Dominko, R., Masquelier, C., Sirisopanaporn, C., Armstrong, A. R., & Bruce, P. G. (2011). Silicate cathodes for lithium batteries: alternatives to phosphates? *Journal of Materials Chemistry*, 9811-9818.

Jansen, A. N., Kahaian, A. J., Kepler, K. D., Nelson, P. A., Amine, K., Dees, D. W., et al. (1999). Development of a high-power lithium-ion battery. *Journal of Power Sources*, 902-905.

Kim, D. K., Muralidharan, P., Lee, H.-W., Ruffo, R., Yang, Y., Chan, C. K., et al. (2008). Spinel LiMn2O4 Nanorods as Lithium Ion Battery Cathodes. *Nano Letters*, 3948-3952.

Leenen, M. A., Arning, V., Thiem, H., Steiger, J., & Anselmann, R. (2009). Printable Electronics: Flexibility for the Future. *Physica Status Solidi A*, 588-597.

Liu, C., Li, F., Ma, L.-P., & Cheng, H.-M. (2010). Advanced Materials for Energy Storage. *Advanced Energy Materials*, E28-E62.

Lu, S. T. (2006, November 22). *Electrochemical studies of low-temperature processed.* Retrieved October 2011, from Sciencedirect: http://my.wpi.edu/webapps/portal/frameset.jsp?tab_id=_2_1&url=%2fwebapps%2fblackboard%2fexecute%2flauncher%3ftype%3dCourse%26id%3d_162526_1%26url%3d

Neudecker, B. J., Dudney, N. J., & Bates, J. B. (2000). "Lithium-Free" Thin-Film Battery with In Situ Plated Li Anode. *Journal of the Electrochemical Society*, 517-523.

Nishi, Y. (2001). Lithium ion secondary batteries; past 10 years and the future. *Journal of Power Sources*, 101-106.

Nishi, Y. (2001). *Lithium Ion Secondary Batteries; Past 10 Years and the Future.* Retrieved September 2011, from Journal of Power Sources: www.elseviar.com/locate/jpowersour

Patterson, M. L. (2009, November 13). *ENERDEL.* Retrieved November 2011, from Indiana University Battery Workshop: http://nano.indiana.edu/documents/MPatterson.pdf

Petrovic, D. (2011, August 23). *Car batteries - impact on environment.* Retrieved November 29, 2011, from Australian Science: http://www.australianscience.com.au/environmental-science/car-batteries-impact-on-environment/

Tarascon, J.-M. (2010). Key Challenges in future Li-battery research. *Philisophical Transactions of the Royal Society*, 3227-3241.

Tarascon, M. A.-M. (2008). *Building Better Batteries.* Nature Publishing Group.

Zhang, X., Ross, J. P., Kostecki, R., Kong, F., Sloop, S., Kerr, J. B., et al. (2001). Diagnostic Characterization of High Power Lithium-Ion Batteries for Use in Hybrid Electric Vehicles. *Journal of the Electrochemical Society*, A463-A470.

Appendices

Appendix A: Carbon Coating SEM Analysis

8% @ 700°C Carbon Coating, SEM Analysis

Spectrum processing :
No peaks omitted

Processing option : All elements analyzed (Normalised)
Number of iterations = 3

Standard :
C CaCO3
O SiO2
Si SiO2
Mn Mn

Element	Weight%	Atomic%
C K	14.82	25.48
O K	40.59	52.40
Si K	14.87	10.94
Mn K	29.72	11.18
Totals	100.00	

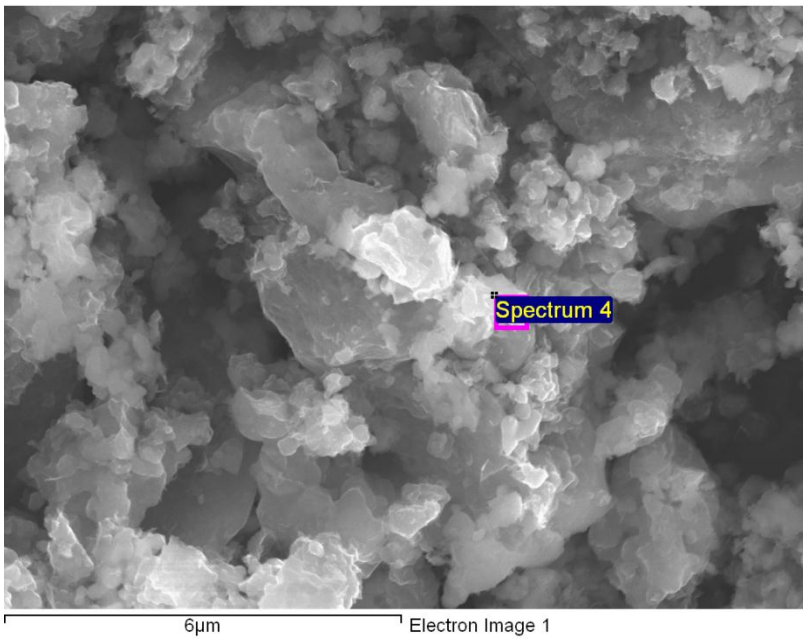

Figure 30: SEM Image of 8% Carbon, Spectrum 4

Comment: At this point in the material, labeled as Spectrum 4 in Figure 30, there is 14.82% carbon on the surface as shown in the EDX image Figure 29.

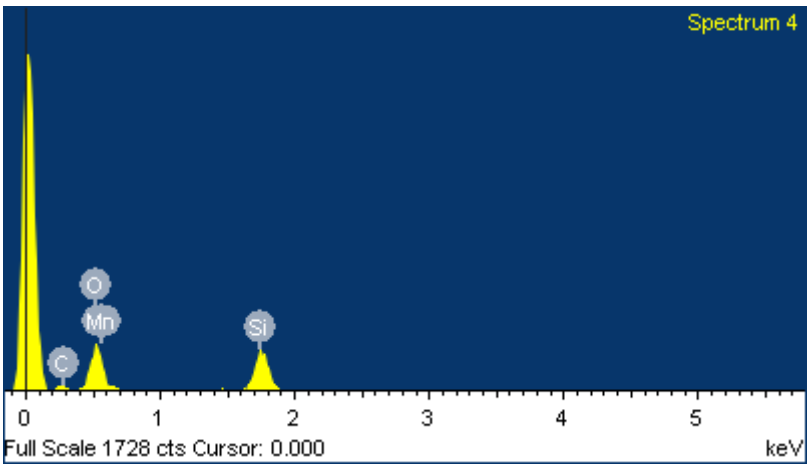

Figure 29: EDX Pattern for 8% Carbon, Spectrum 4

8% @ 700°C Carbon Coating, SEM Analysis

Spectrum processing :
No peaks omitted

Processing option : All elements analyzed (Normalised)
Number of iterations = 3

Standard :
C CaCO3
O SiO2
Si SiO2
Mn Mn

Element	Weight%	Atomic%
C K	7.06	11.91
O K	52.60	66.60
Si K	18.76	13.53
Mn K	21.59	7.96
Totals	100.00	

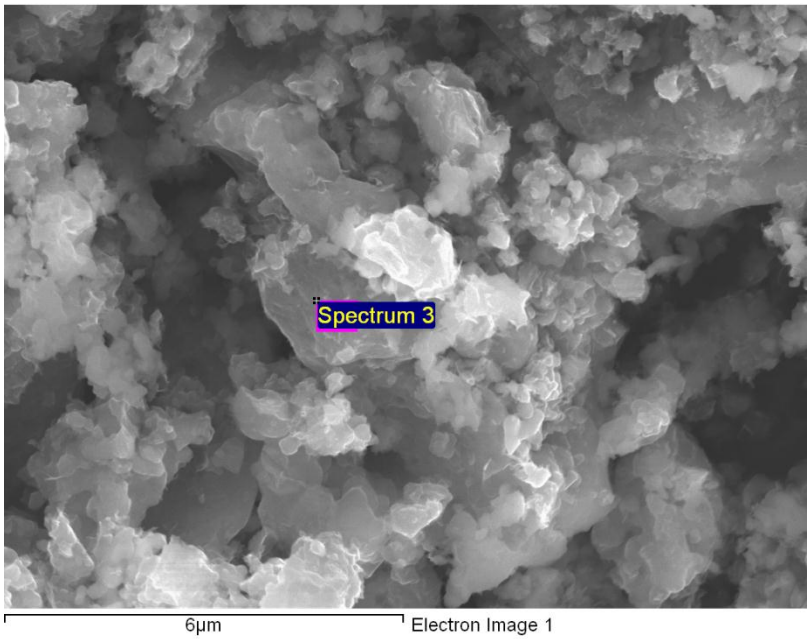

Figure 32: SEM Image of 8% Carbon, Spectrum 3

Comment: At this point on the material, labeled as Spectrum 3 in Figure 32, there was less carbon on the surface than at point Spectrum 4 in Figure 30, at 7.06wt% as shown in the EDX image, Figure 31.

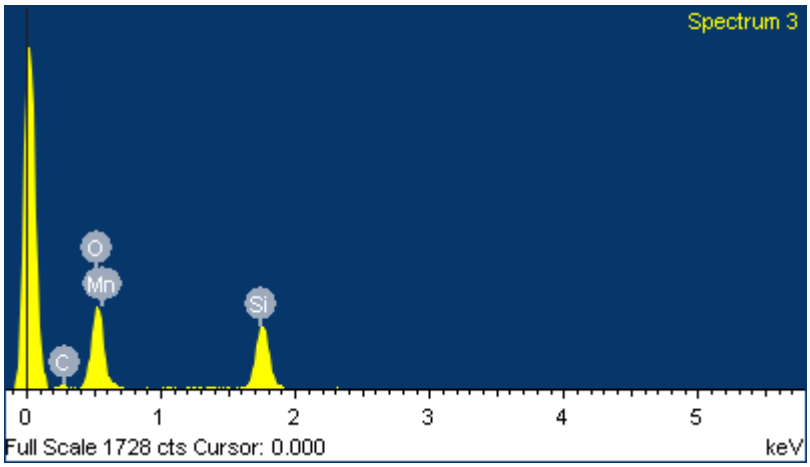

Figure 31: EDX Pattern for 8% Carbon, Spectrum 3

8% @ 700°C Carbon Coating, SEM Analysis

Spectrum processing :
No peaks omitted

Processing option : All elements analyzed (Normalised)
Number of iterations = 4

Standard :
C CaCO3
O SiO2
Si SiO2
Mn Mn

Element	Weight%	Atomic%
C K	14.96	23.75
O K	49.96	59.53
Si K	13.71	9.31
Mn K	21.36	7.41
Totals	100.00	

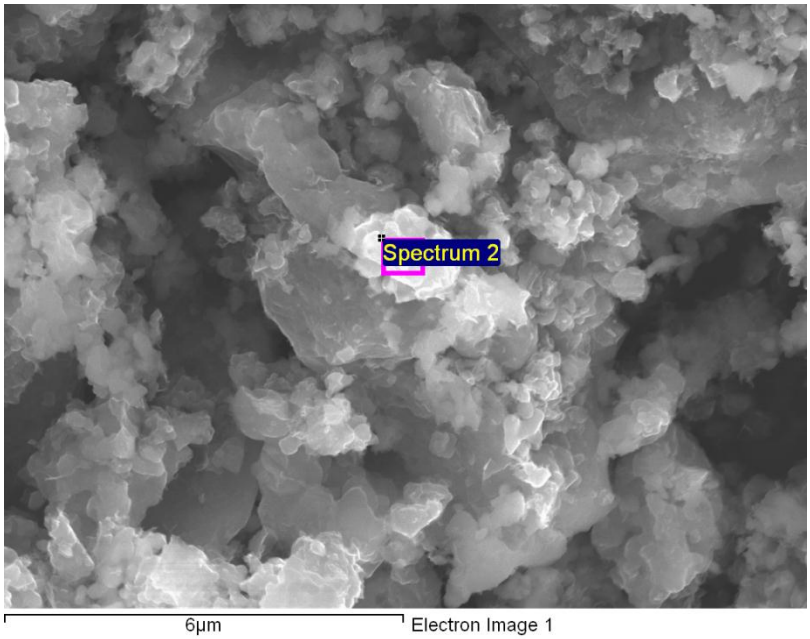

Figure 34: SEM Image of 8% Carbon, Spectrum 2

Comment: At this point in the material, labeled as Spectrum 2 in Figure 34, there is approximately the same amount of carbon on this point as there is on point Spectrum 4 in Figure 30, at 14.96wt%, as shown in EDX image, Figure 33.

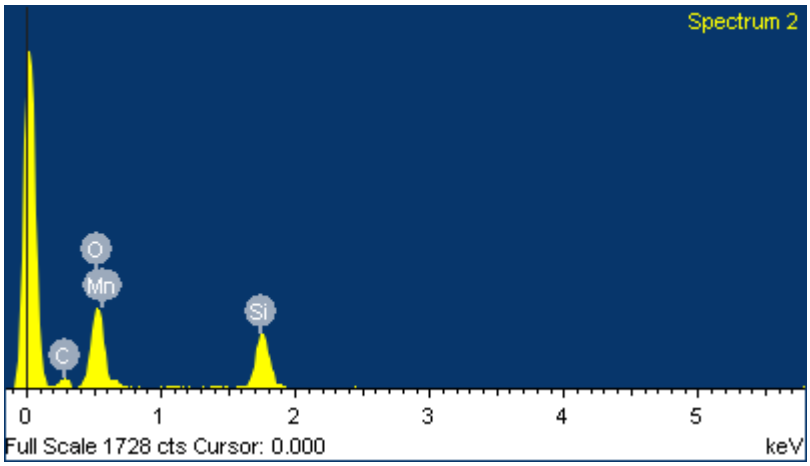

Figure 33: EDX Pattern for 8% Carbon, Spectrum 2

10% @ 700°C Carbon Coating, SEM Analysis

Spectrum processing :
No peaks omitted

Processing option : All elements analyzed (Normalised)
Number of iterations = 4

Standard :
C CaCO3
O SiO2
Si SiO2
Mn Mn

Element	Weight%	Atomic%
C K	17.27	27.09
O K	47.77	56.27
Si K	14.18	9.51
Mn K	20.78	7.13
Totals	100.00	

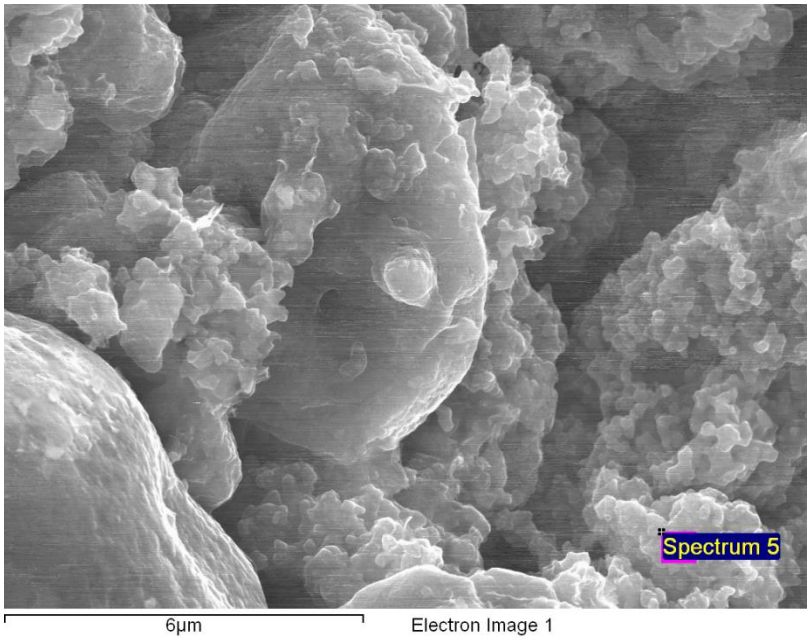

Figure 36: SEM Image of 10% Carbon, Spectrum 5

Comment: Point Spectrum 5 in Figure 36 depicts a point with 17.27wt% carbon as shown in EDX image Figure 35.

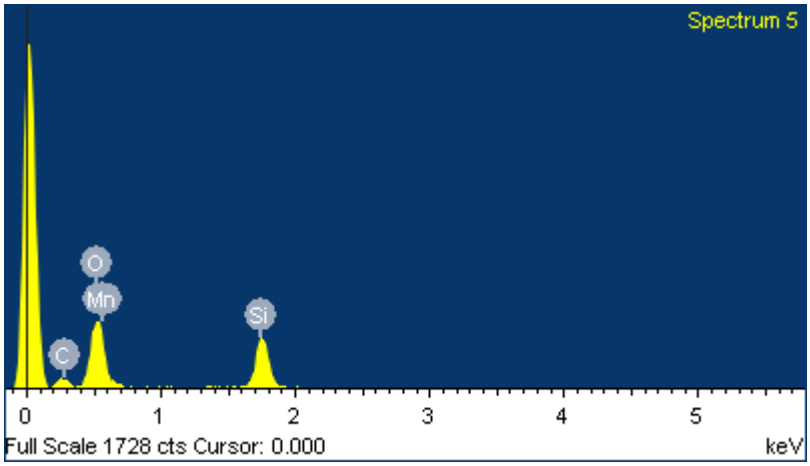

Figure 35: EDX Pattern for 10% Carbon, Spectrum 5

10% @ 700°C Carbon Coating, SEM Analysis

Spectrum processing :
No peaks omitted

Processing option : All elements analyzed (Normalised)
Number of iterations = 4

Standard :
C CaCO3
O SiO2
Si SiO2
Mn Mn

Element	Weight%	Atomic%
C K	16.13	25.29
O K	47.46	55.89
Si K	19.32	12.96
Mn K	17.09	5.86
Totals	100.00	

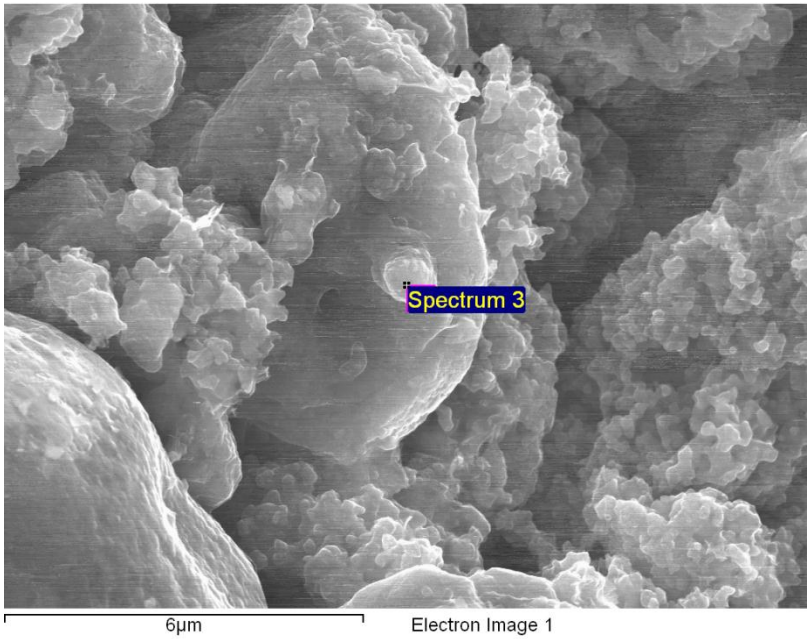

Figure 38: SEM Image of 10% Carbon, Spectrum 3

Comment: Point Spectrum 3 in Figure 38 indicates the point where the carbon coating is at 16.13wt% as shown in EDX image Figure 37

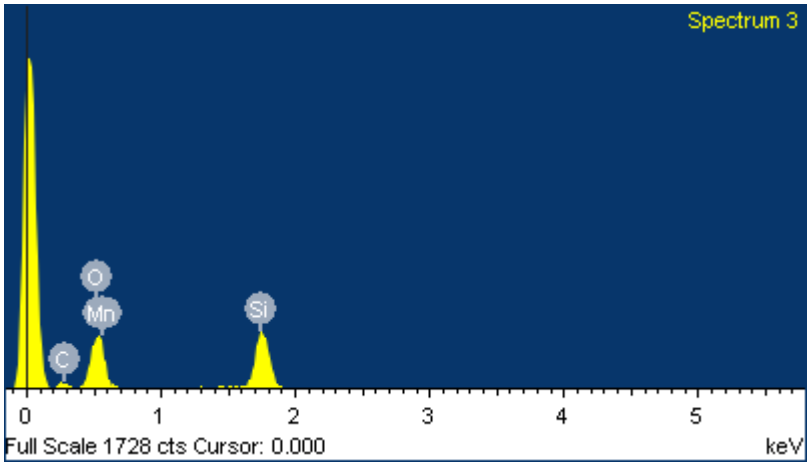

Figure 37: EDX Pattern for 10% Carbon, Spectrum 3

10% @ 700°C Carbon Coating, SEM Analysis

Spectrum processing :
No peaks omitted

Processing option : All elements analyzed (Normalised)
Number of iterations = 4

Standard :
C CaCO3
O SiO2
Si SiO2
Mn Mn

Element	Weight%	Atomic%
C K	16.71	27.03
O K	45.36	55.10
Si K	13.15	9.10
Mn K	24.78	8.77
Totals	100.00	

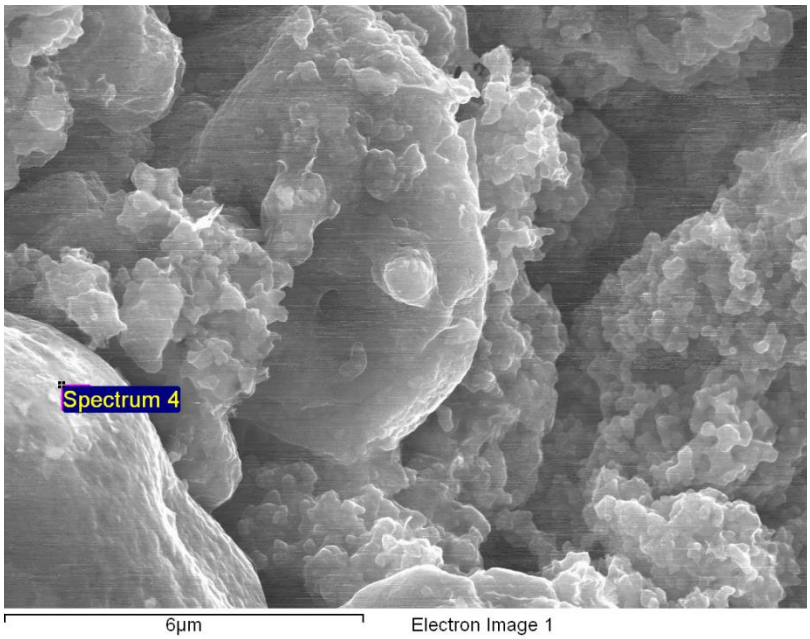

Figure 40: SEM Image of 10% Carbon, Spectrum 4

Comment: Point Spectrum 4 indicates a point at which carbon is 16.71wt% as shown in EDX image Figure 39.

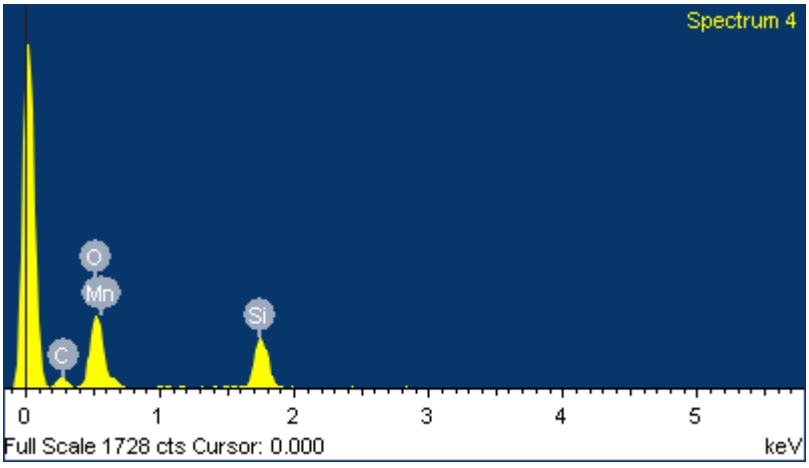

Figure 39: EDX Pattern for 10% Carbon, Spectrum 4

10% @ 700°C Carbon Coating, SEM Analysis

Spectrum processing :
No peaks omitted

Processing option : All elements analyzed (Normalised)
Number of iterations = 4

Standard :
C CaCO3
O SiO2
Si SiO2
Mn Mn

Element	Weight%	Atomic%
C K	15.91	25.11
O K	49.26	58.38
Si K	13.62	9.19
Mn K	21.21	7.32
Totals	100.00	

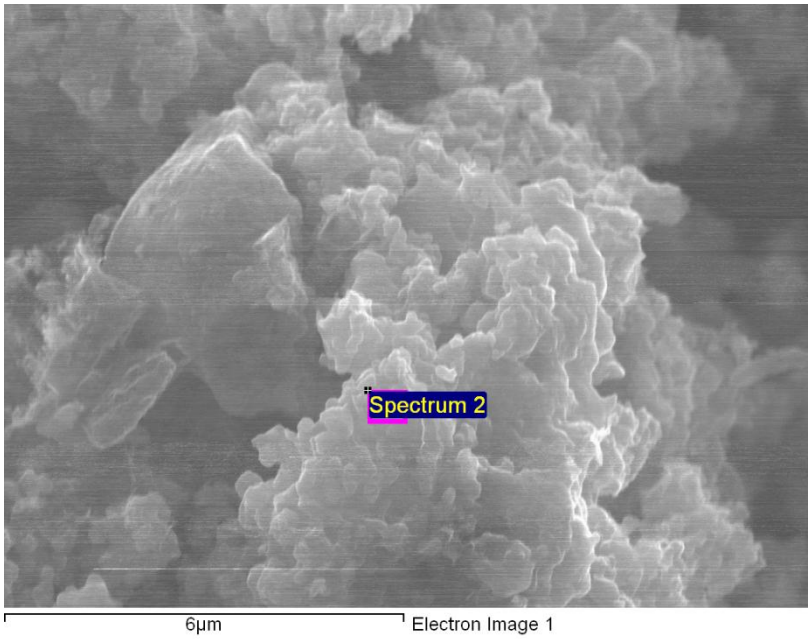

Figure 42: SEM Image of 10% Carbon, Spectrum 2

Comment: Point Spectrum 2 in Figure 42 indicates a point that is coated with 15.91wt% carbon as shown in EDX image Figure 41.

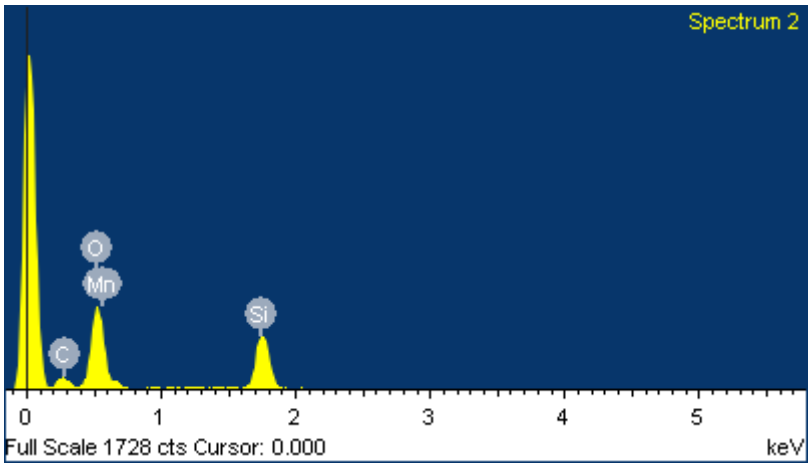

Figure 41: EDX Pattern for 10% Carbon, Spectrum 2

10% @ 700°C Carbon Coating, SEM Analysis

Spectrum processing :
No peaks omitted

Processing option : All elements analyzed (Normalised)
Number of iterations = 4

Standard :
C CaCO3
O SiO2
Si SiO2
Mn Mn

Element	Weight%	Atomic%
C K	11.42	18.32
O K	53.62	64.62
Si K	14.28	9.80
Mn K	20.69	7.26
Totals	100.00	

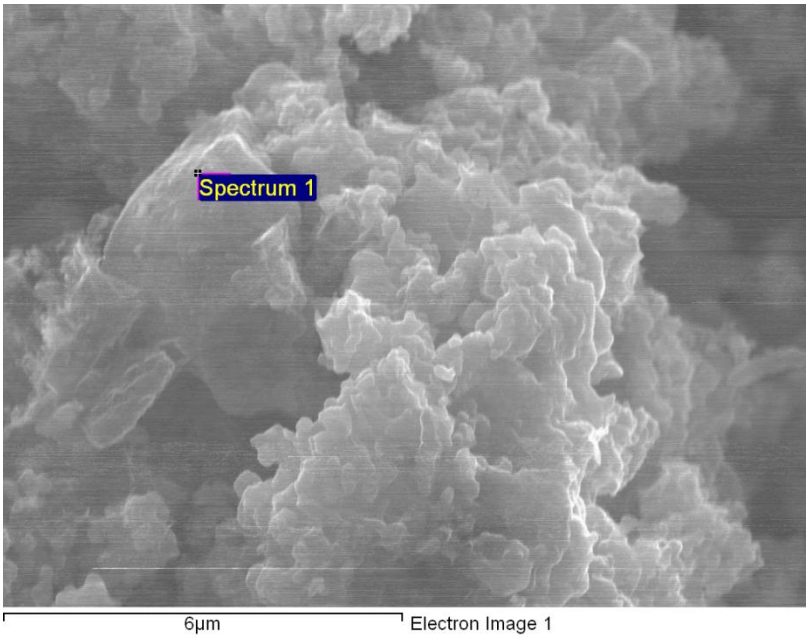

Figure 44: SEM Image of 10% Carbon, Spectrum 1

Comment: Point Spectrum 1 indicates the least amount of carbon coating in the 10% carbon coating sample at 11.42wt% as shown in EDX image Figure 43

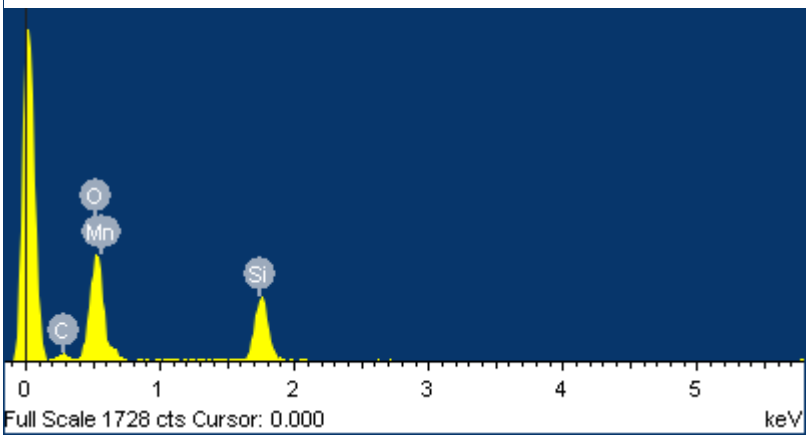

Figure 43: EDX Pattern for 10% Carbon, Spectrum 1

12% @ 700°C Carbon Coating, SEM Analysis

Spectrum processing :
No peaks omitted

Processing option : All elements analyzed (Normalised)
Number of iterations = 4

Standard :
C CaCO3
O SiO2
Si SiO2
Mn Mn

Element	Weight%	Atomic%
C K	18.74	29.79
O K	43.92	52.41
Si K	14.53	9.88
Mn K	22.80	7.92
Totals	100.00	

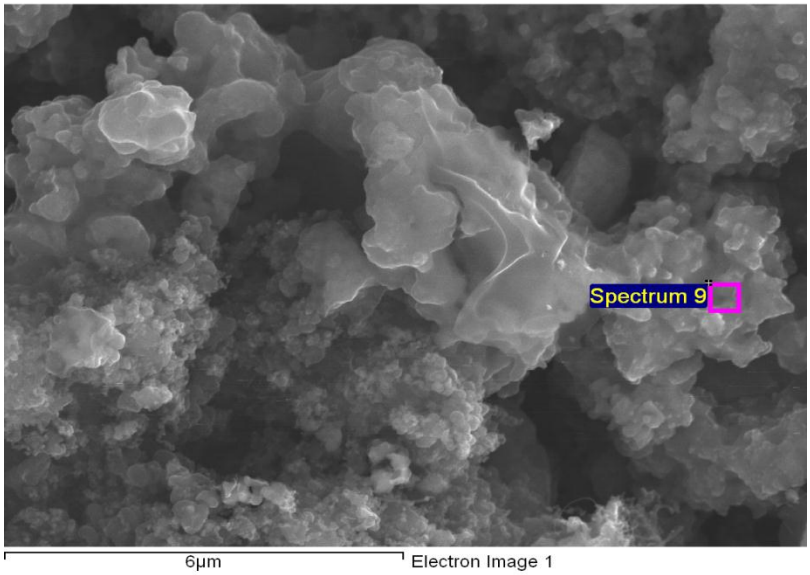

Figure 46: SEM Image of 12% Carbon, Spectrum 9

Comment: Point Spectrum 9 in Figure 46 of the 12% carbon coating indicates a 18.74wt% carbon layer on the test material.

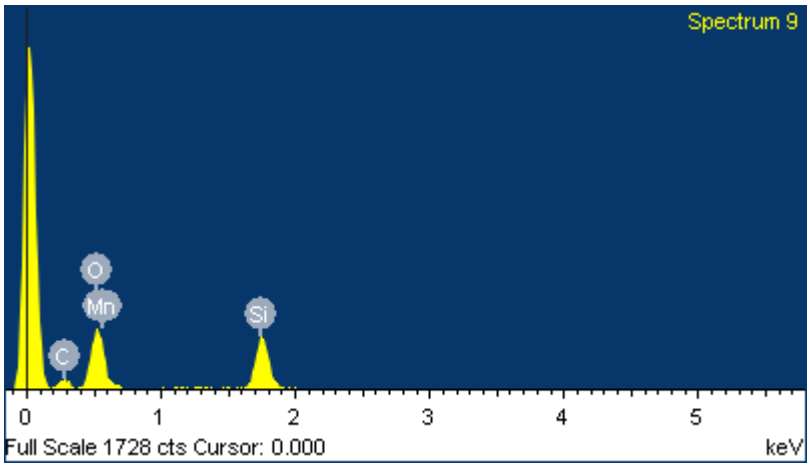

Figure 45: EDX Pattern for 12% Carbon, Spectrum 9

12% @ 700°C Carbon Coating, SEM Analysis

Spectrum processing :
No peaks omitted

Processing option : All elements analyzed (Normalised)
Number of iterations = 4

Standard :
C CaCO3
O SiO2
Si SiO2
Mn Mn
Fe Fe

Element	Weight%	Atomic%
C K	60.49	73.39
O K	23.84	21.71
Si K	2.96	1.53
Mn K	9.79	2.60
Fe K	2.92	0.76
Totals	100.00	

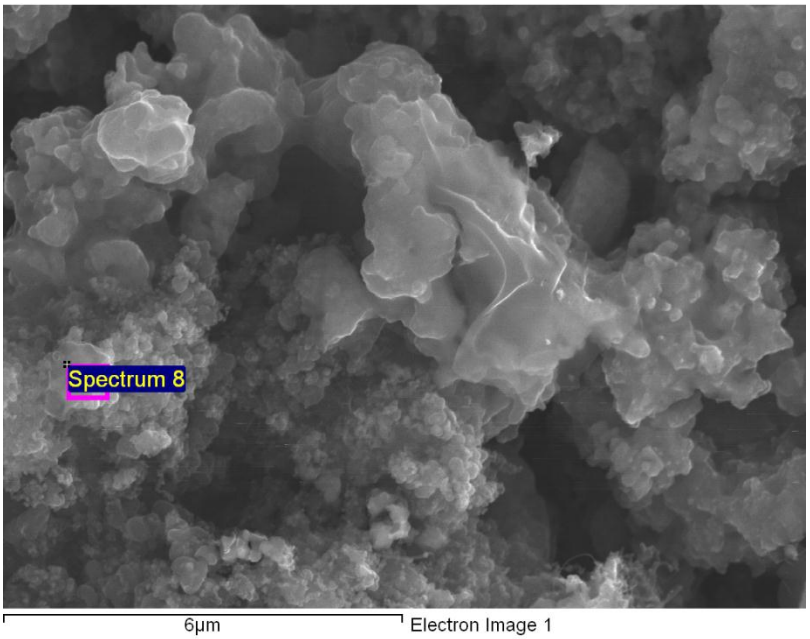

Figure 48: SEM Image of 12% Carbon, Spectrum 8

Comment: There is much more carbon on the surface of point Spectrum 8 in Figure 48, at 60.49wt%, as shown in EDX image Figure 47.

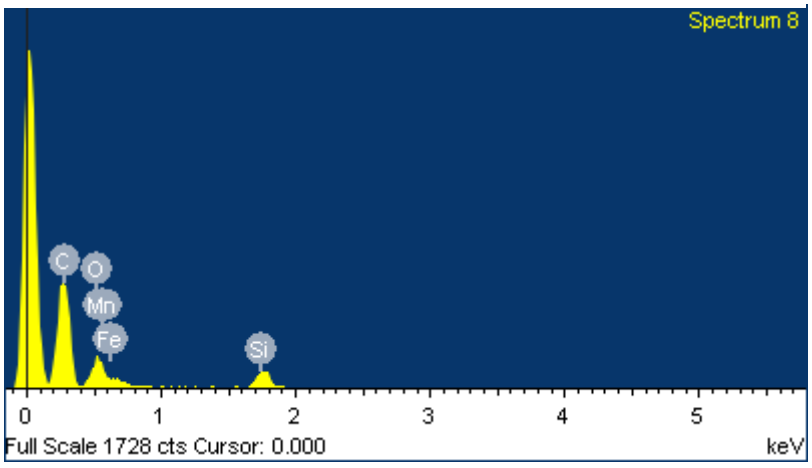

Figure 47: EDX Pattern for 10% Carbon, Spectrum 8

12% @ 700°C Carbon Coating, SEM Analysis

Spectrum processing :
No peaks omitted

Processing option : All elements analyzed (Normalised)
Number of iterations = 4

Standard :
C CaCO3
O SiO2
Si SiO2
Mn Mn

Element	Weight%	Atomic%
C K	27.48	40.41
O K	42.42	46.82
Si K	10.08	6.34
Mn K	20.02	6.43
Totals	100.00	

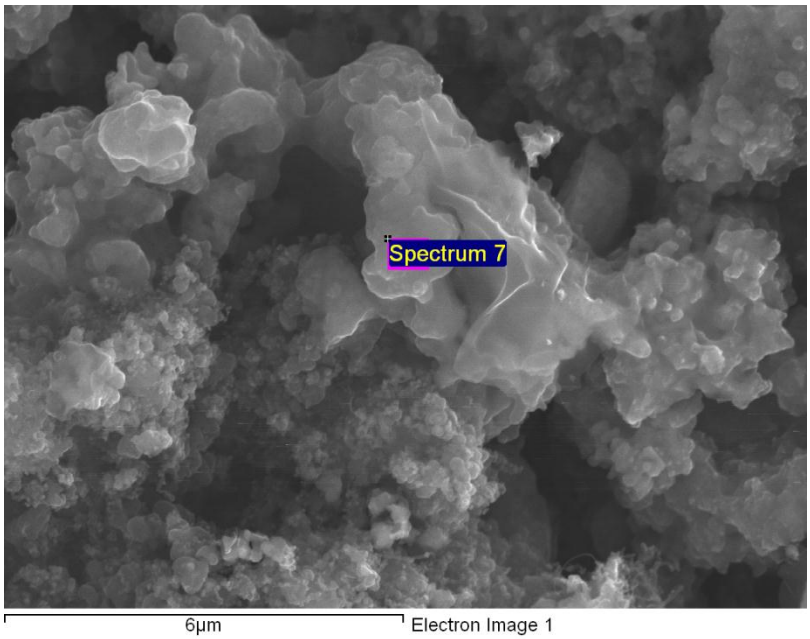

Figure 50: SEM Image of 12% Carbon, Spectrum 7

Comment: Point Spectrum 7 in Figure 50 has less carbon than Figure 48, but more than Figure 46, at 27.48wt% as shown in Figure 49.

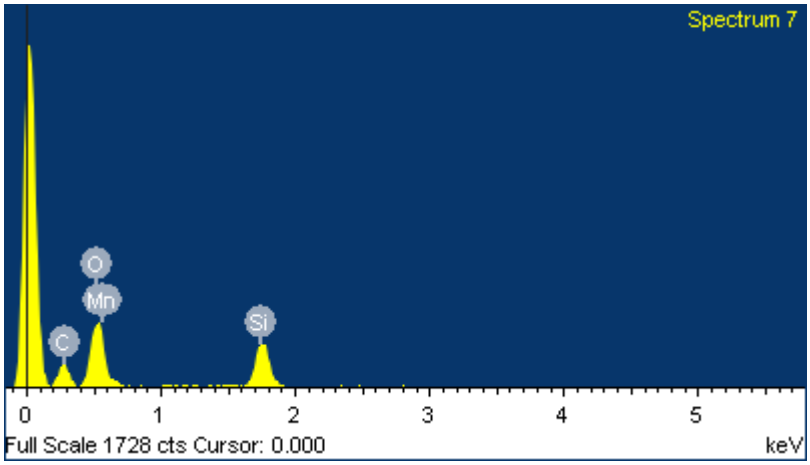

Figure 49: EDX Pattern for 10% Carbon, Spectrum 7

Appendix B: Electrochemical Data

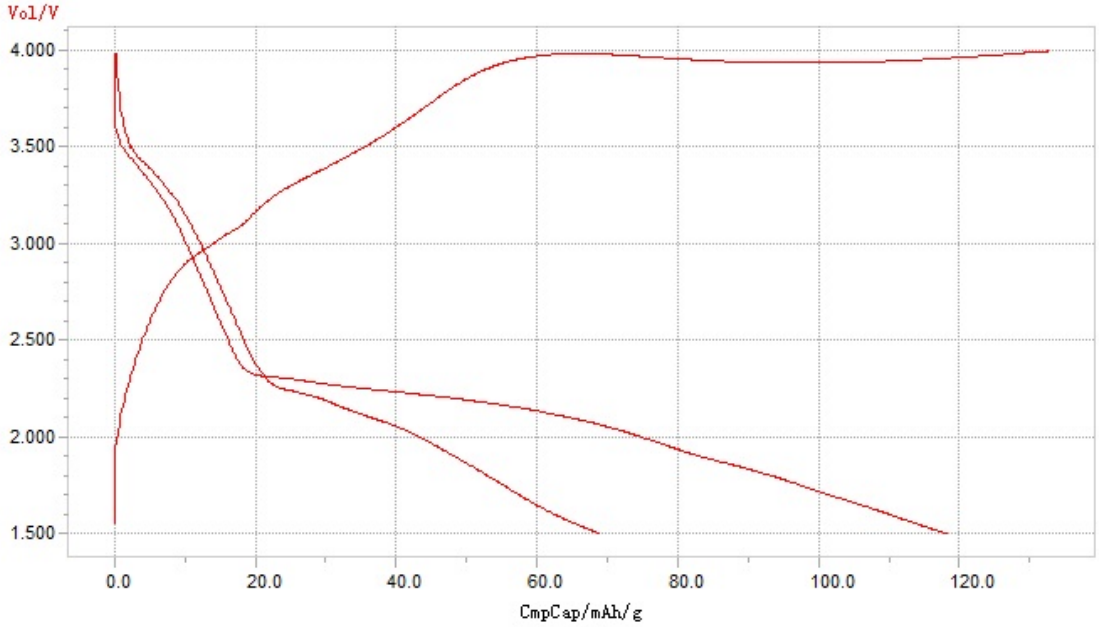

Figure 51: Fe70/Mn30 Coin-Cell Data 20 Cycles

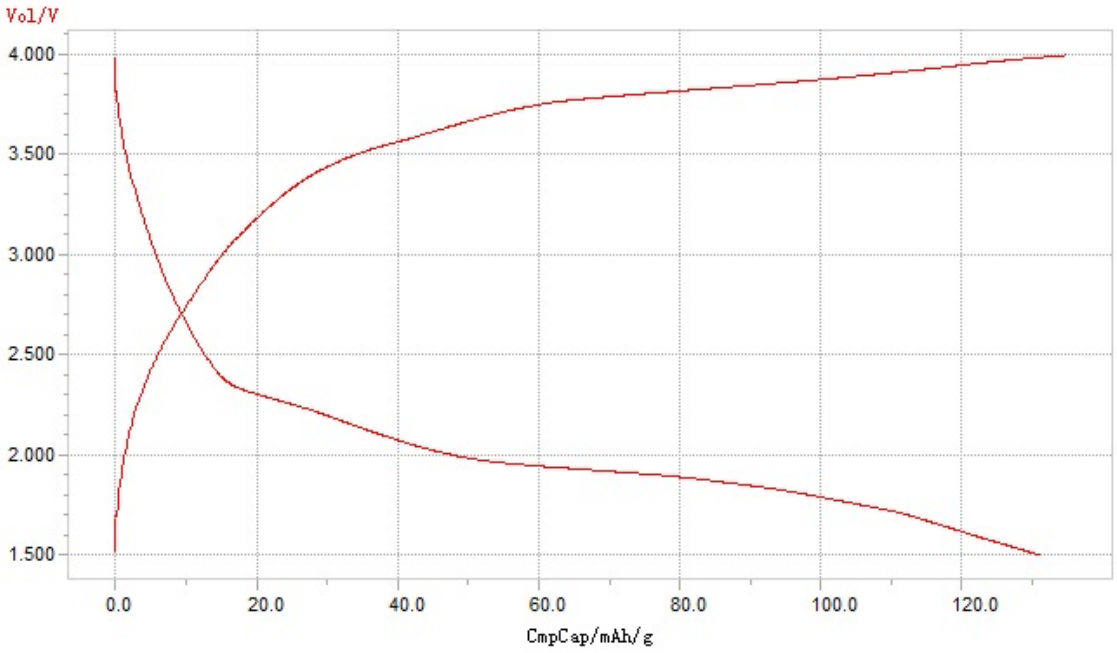

Figure 52: Fe50/Mn50 Coin-Cell Data

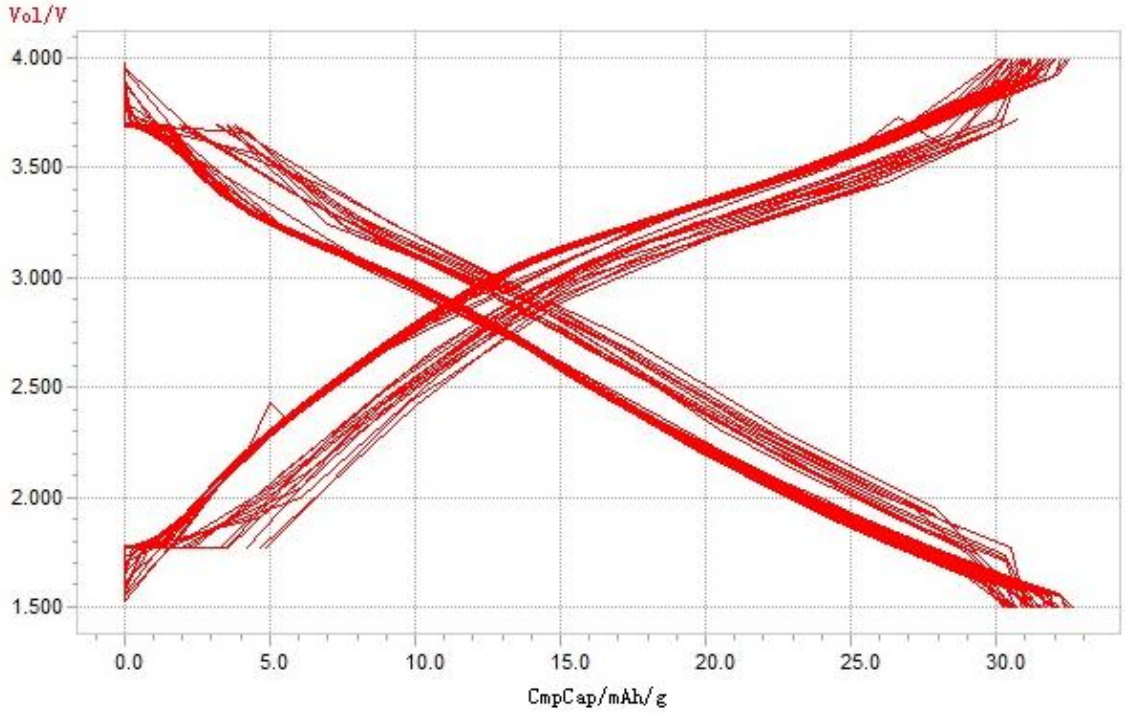

Figure 53: Fe70/Mn30 W/ Carbon Coin-Cell Data 20 Cycles

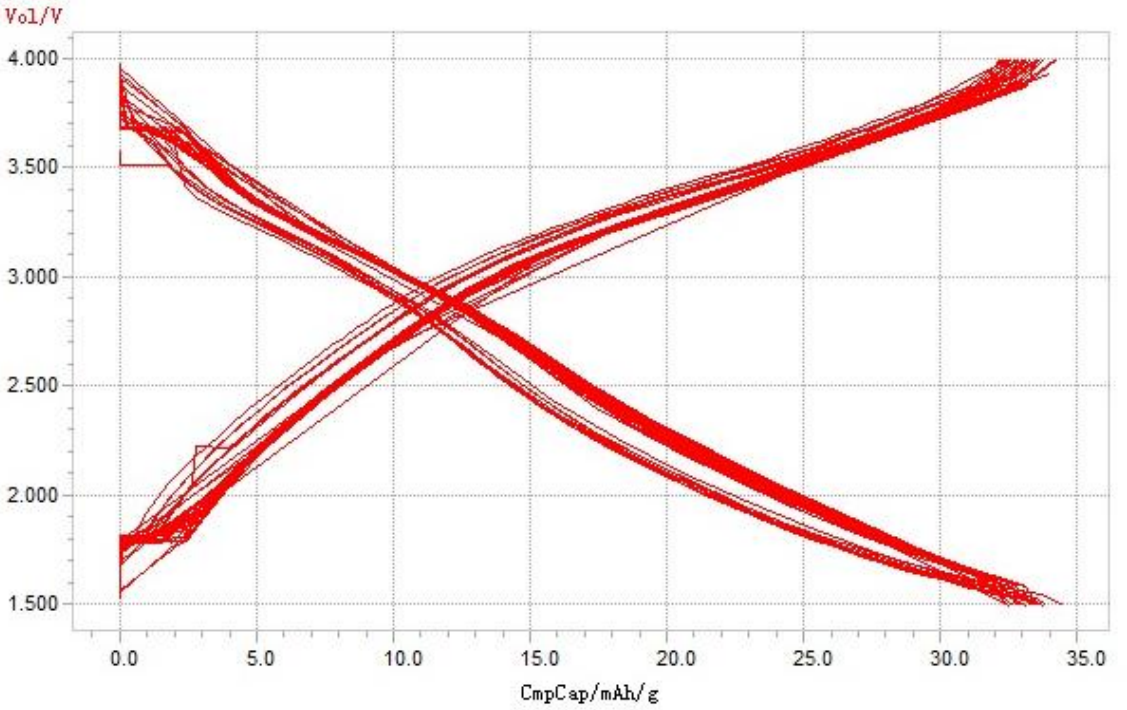

Figure 54: Fe50/Mn50 W/ Carbon Coin-Cell Data 20 Cycles

Appendix C: Stepwise Procedure

Cathode Synthesis:

1. Weigh out $FeC_2O_4 \cdot 2H_2O$ and $LiCH_3COO \cdot 2H_2O$ according to the weights listed in Table 1 and add both reagents to a 125mL Erlenmeyer flask
2. Add 20mL of ethanol to the flask
3. Insert a magnetic stirring bar to the flask and place on top of a stirring plate
4. Place a rubber stopper with a pipette inserted through the center on top of the flask
5. Attach the tubing used to deliver the nitrogen flux to the pipette (see Figure 10)
6. Turn on the stirring plate and set the speed to a medium setting
7. Turn on the nitrogen flux
8. After $FeC_2O_4 \cdot 2H_2O$ and $LiCH_3COO \cdot 2H_2O$ solution is fully dissolved, using a pipette, add 5mL of tetraethyl orthosilicate dropwise through the exhaust hole on the side of the flask
9. Weigh out 4.60g of $LiCH_3COO \cdot 2H_2O$ and add to a 50mL beaker
10. Add 20mL of ethanol to the beaker
11. Insert a magnetic stirring bar into the beaker and seal the top with parafilm
12. Place the beaker on top of stirring plate
13. Turn on the stirring plate and set the speed to a high setting
14. Using a pipette, add the lithium solution dropwise through the exhaust hole on the side of the $FeC_2O_4 \cdot 2H_2O$, $LiCH_3COO \cdot 2H_2O$, tetraethyl orthosilicate containing flask
15. Using a pipette, add 0.5mL of D.I. water dropwise through the exhaust hole on the side of the flask
16. Using a pipette, add 1.5mL of acetic acid dropwise through the exhaust hole on the side of the flask
17. Adjust the stirring speed to a mild setting and let the solution stir for at least 6 hours
18. Using a metal spatula, remove the gel from the flask and transfer to a ceramic beaker.
19. Place the ceramic boat in the tube furnace
20. Attach the gas tubes to each end of the quartz tube and turn on the nitrogen flux
21. Set the furnace to 80^oC and heat for 24 hours
22. Using a spatula, remove the dry gel and transfer to a mortar
23. Using a pestle, grind the material into a fine powder
24. *If carbon coating is desired, see the procedure below
25. Transfer the powder to the crimping machine
26. Set the machine to apply 20,000 lbs_f for 2 minutes
27. Transfer the pellet to the ceramic boat and place inside the tube furnace
28. Attach the gas tubes to each end of the quartz tube and turn on the nitrogen flux
29. Set the furnace to a heating rate of 10^oC per minute until a temperature of 300^oC is reached
30. After 300^oC, set the furnace to a heating rate of 2^oC per minute until a final temperature of 700^oC is reached
31. Heat the pellet at 700^oC for 10 hours

32. Remove the pellet from the tube furnace and transfer it to a mortar
33. Using a pestle, grind the pellet into a fine powder

Carbon Coating:

1. Using a metal spatula, transfer the powder from step 21 above to a scale and weigh out the material
2. Weigh out 10% of the weight of the powder in commercial sucrose
3. Transfer the commercial sucrose to a mortar
4. Using a pestle, grind the commercial sucrose to a fine powder
5. Add the powder and commercial sucrose to a 50mL beaker
6. Add 15mL of acetone to the beaker
7. Insert a magnetic stirring bar into the beaker and seal the top with parafilm
8. Place the beaker on top of stirring plate
9. Turn on the stirring plate and set the speed to a medium setting
10. After stirring for 3 hours, remove the stirring bar from beaker
11. Remove the parafilm from the top of beaker and replace it with a piece of aluminum foil
12. Poke a few small holes in the top of the aluminum foil
13. Transfer the beaker to the box furnace
14. Set the box furnace to 70^{o}C and heat for 24 hours
15. Transfer the dry material to a mortar
16. Using a pestle, grind the material into a fine powder
17. To calcinate the carbon coated material, follow steps 23-31 above

Coin Cell Assembly:

1. Using a spatula, transfer the powder from step 31 to a scale and weigh out the material
2. Weigh out 12.5% of the weight of the powder in poly(vinylidene fluoride) and in carbon black
3. For every 0.02g of poly(vinylidene fluoride) weighed out in the step above, measure 1mL of N-methyl-2-pyrrolidene
4. Add the poly(vinylidene fluoride) and N-methyl-2-pyrrolidene to a 20mL capped bottle
5. Insert a magnetic stirring bar into the bottle and screw the cap on top
6. Place the bottle on top of stirring plate
7. Turn on the stirring plate and set the speed to a high setting
8. Stir the solution for 3 hours
9. Add the powder from step 31 and carbon black to the poly(vinylidene fluoride) and N-methyl-2-pyrrolidene containing bottle
10. Adjust the stirring speed to a mild setting and let the slurry stir for 2 hours
11. Using a ½" puncher, cut out a circular piece of aluminum foil

12. Using sand paper, scrape the surface of the aluminum foil
13. Sonicate the aluminum foil in a 50% ethanol 50% acetone bath
14. Air dry the aluminum foil and transfer it to a scale
15. Measure the weight of the aluminum foil and record it
16. Transfer the aluminum foil onto a hot plate
17. Using a pipette, place 4 drops of the cathode material, poly(vinylidene fluoride), carbon black and N-methyl-2-pyrrolidene slurry onto the aluminum foil
18. Turn on the hot plate and set the temperature to 60°C
19. After the coated aluminum foil is dry, transfer it to the scale
20. Measure the weight of the coated aluminum foil and subtract the weight of the bare aluminum foil to find the weight of the active material
21. Transfer the coated aluminum foil to the vacuum oven
22. Set the vacuum oven to a temperature of 120°C and heat for 10 hours
23. Using a ¾" puncher, cut out a circular piece of polypropylene separator
24. Using a ½" puncher, cut out a circular piece of lithium foil
25. Transfer the coated aluminum foil current collector, polypropylene separator, $LiPF_6$, ethylene carbonate, ethyl methyl carbonate, lithium foil, spacer, spring and both sides of the coin cell casing to the vacuum glove box
26. Set the glove box to operate at an H_2O level of <0.1ppm and an O_2 level of <4.6ppm
27. Inside the glove box mix the $LiPF_6$, ethylene carbonate and ethyl methyl carbonate in a 1:1:1 ratio to create the electrolyte solution
28. Using non-metal tweezers, place the coated aluminum current collector on top of the cathode side of the coin cell casing (see Figure 55)
29. Using non-metal tweezers, stack the polypropylene separator on top of the coated aluminum foil current collector
30. Using a pipette, drop 4 drops of the electrolyte solution onto the separator
31. Using non-metal tweezers, stack the lithium foil on top of the electrolyte covered separator
32. Using non-metal tweezers, stack the spacer on top of the lithium foil
33. Using non-metal tweezers, stack the spring on top of the spacer
34. Seal the coin cell by placing the anode side of the coin cell shell on top of the spacer
35. Pretest the cell with a voltmeter
36. Remove the coin cell from the glove box
37. Transfer the coin cell to the crimping machine
38. Set the machine to 1000psi for 15 seconds
39. Attach the newly assembled coin cell to the battery test station and begin electrochemical testing

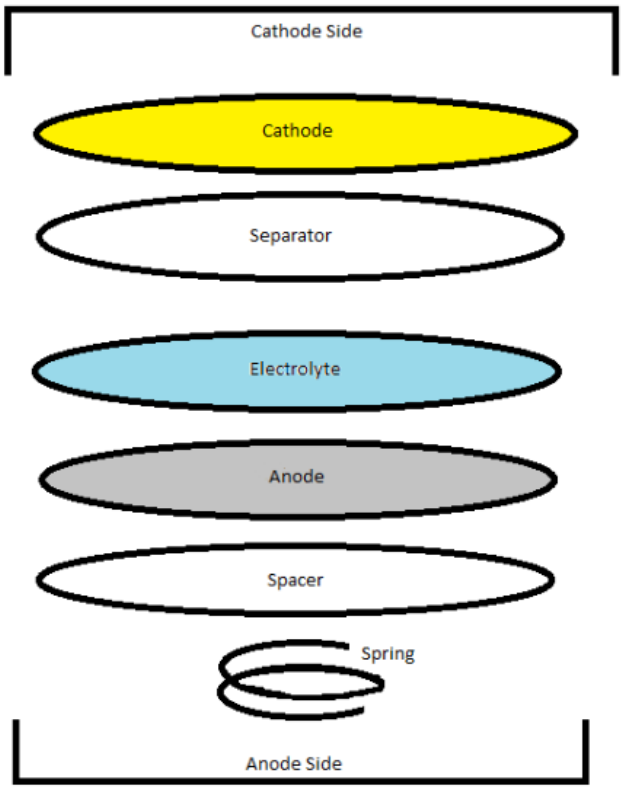

Figure 55: Exploded Coin Cell Assembly Diagram

Appendix D: Project Components

Table 2: List of Chemical Reagents

Name	Brand and Purity
Lithium acetate dehydrate ($LiCH_3COO•2H_2O$)	Alfa Aesar, 99%
Iron oxalate dehydrate ($FeC_2O_4•2H_2O$)	Alfa Aesar, 99%
Manganese acetate tetrahydrate ($Mn(CH_3COO)_2•4H_2O$)	Alfa Aesar, Mn 22%
Tetraethyl orthosilicate (TEOS)	Aldrich, Reagent Grade, 98%
Lithium Hexafluorophosphate ($LiPF_6$)	Syerm Chemicals, INC, 99.9%+
Ethylene carbonate (EC)	ACROS, 99%+
Ethyl Methyl Carbonate (EMC)	ACROS, 99%+
Poly(vinylidene fluoride) (PVDF)	Alfa Aesar
N-methyl-2-pyrrolidene (NMP)	Sigma-Aldrich, 99.5%
Carbon Black (CB)	Alfa Aesar, 99%+
Nitrogen (N_2)	AIMTEK, 99.999%
Lithium foil	Alfa Aesar, 99.9%
Aluminum foil	Alfa Aesar, 99.9%
Commercial sucrose	Great Value

Table 2 lists the chemicals used throughout the project, as well as the brand and purity.

Table 3: List of Instruments

Instrument	Model
Tube Furnace	Thermolyne 79300
Vacuum Oven	Precision Scientific Model 19
Glove Box	
SEM	JSM – 7000F
XRD	X'PERT POWDER
Battery Test Station	MTI-EQ-BST8-10MA
Coin Cell Shell	CR2032
Separator	Celgard® 2500
Puncher	
Compact Hydraulic Crimping Machine	MSK-110
Scale	Mettler Toledo AB54-S/FACT
Stirring Plate/Hot plate	Corning Hot Plate Stirrer PC-351
Sonicator	Branson 2510
Box furnace	Thermolyne FB1415M
Stirring Plate	Fisher Scientific Isotemp
Volt Meter	Omega HHM26

Table 3 lists the instruments used throughout the project, as well as the model number of each.

Table 4: List of Tools

Tools	Quantity
125 mL Erlenmeyer flask	1
50 mL graduated cylinder	1
Magnetic stirring bar	1
Chemical spatula	3
Glass pipette	1
50 mL beaker	1
Pestle & mortar	1
Ceramic boat	2
Parafilm	N/A

Table 4 lists the tools used throughout the project.